Accepted Manuscript

Targeting heme Oxygenase-1 with hybrid compounds to overcome Imatinib resistance in chronic myeloid leukemia cell lines

Valeria Sorrenti, Valeria Pittalà, Giuseppe Romeo, Emanuele Amata, Maria Dichiara, Agostino Marrazzo, Rita Turnaturi, Orazio Prezzavento, Ignazio Barbagallo, Luca Vanella, Antonio Rescifina, Giuseppe Floresta, Daniele Tibullo, Francesco Di Raimondo, Sebastiano Intagliata, Loredana Salerno

PII: S0223-5234(18)30820-1

DOI: 10.1016/j.ejmech.2018.09.048

Reference: EJMECH 10759

To appear in: *European Journal of Medicinal Chemistry*

Received Date: 1 August 2018

Revised Date: 14 September 2018

Accepted Date: 15 September 2018

Please cite this article as: V. Sorrenti, V. Pittalà, G. Romeo, E. Amata, M. Dichiara, A. Marrazzo, R. Turnaturi, O. Prezzavento, I. Barbagallo, L. Vanella, A. Rescifina, G. Floresta, D. Tibullo, F. Di Raimondo, S. Intagliata, L. Salerno, Targeting heme Oxygenase-1 with hybrid compounds to overcome Imatinib resistance in chronic myeloid leukemia cell lines, *European Journal of Medicinal Chemistry* (2018), doi: https://doi.org/10.1016/j.ejmech.2018.09.048.

Targeting Heme Oxygenase-1 with Hybrid Compounds to Overcome Imatinib Resistance in Chronic Myeloid Leukemia Cell Lines

Valeria Sorrenti [a], Valeria Pittalà [a,*], Giuseppe Romeo [a], Emanuele Amata [a], Maria Dichiara [a], Agostino Marrazzo [a], Rita Turnaturi [a], Orazio Prezzavento [a], Ignazio Barbagallo [a], Luca Vanella [a], Antonio Rescifina [a], Giuseppe Floresta [a, b], Daniele Tibullo [c, d], Francesco Di Raimondo [c], Sebastiano Intagliata [e], Loredana Salerno [a,*].

[a] Department of Drug Sciences, University of Catania, viale A. Doria 6, 95125, Catania, Italy.

[b] Department of Chemical Sciences, University of Catania, viale A. Doria 6, 95125, Catania, Italia.

[c] Division of Hematology, A.O.U. Policlinico-OVE, University of Catania, via S. Sofia, 78, 95123, Catania, Italy.

[d] Department of Biomedical and Biotechnological Sciences, University of Catania, via S. Sofia, 78, 95123, Catania, Italy.

[e] Department of Medicinal Chemistry, College of Pharmacy, University of Florida, Gainesville, FL, USA.

Corresponding Authors:

Loredana Salerno; l.salerno@unict.it

Valeria Pittalà; vpittala@unict.it

Graphical Abstract

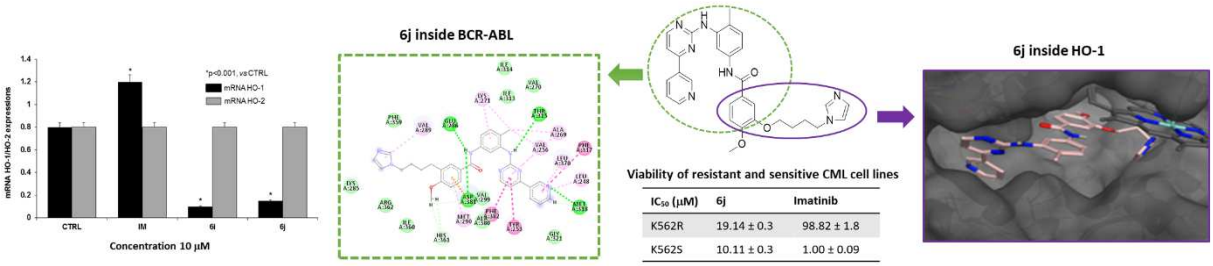

Highlights

- New HO-1/BCR-ABL inhibitors have been synthesized
- Many hybrids are able to inhibit the enzymatic activity of both targets
- The hybrids overcome tyrosine kinase inhibitors resistance
- The hybrids reduce viability of Chronic Myeloid Leukemia Imatinib resistant cells

Keywords: HO-1 inhibitors, Tyrosine kinase inhibitors, BCR-ABL, Imatinib, Chronic myeloid leukemia

Abstract

Heme oxygenase-1 (HO-1) is a cytoprotective enzyme and a survival-enhancing factor in a number of cancers. Chronic myeloid leukemia (CML) is a blood cancer caused by pathological kinase activity of the BCR-ABL protein, currently treated with tyrosine kinase inhibitors (TKIs) such as Imatinib (IM). However, resistance to TKIs persists in a number of patients and HO-1 overexpression has been linked with the induction of chemoresistance in CML. With this in mind, in this study, we designed and synthesized the first series of hybrid compounds obtained by combining the structures of IM, as BCR-ABL inhibitor, with imidazole-based HO-1 inhibitors. We found that many hybrids were able to inhibit the enzymatic activity of both targets and to reduce the

viability of CML IM resistant cells, showing that a single molecular entity may reduce the resistance phenomenon.

1. Introduction

Heme oxygenases (HOs) are enzymes which catalyze the catabolism of heme into free iron, carbon monoxide (CO), and biliverdin, this last successively reduced to bilirubin [1–3]. The main consequence of this enzymatic activity is a cyto-protective effect in various stress-related conditions [4,5]. Three isoforms of HO are present in humans, but only two are enzymatically active: HO-1, which is inducible, and HO-2, which is constitutive. The latter is ubiquitous and is mainly responsible for physiological effects. HO-1, also known as heat shock protein 32 (Hsp32), is found in tissue at low levels with a major presence in the spleen and in the liver, but it may be induced in many other organs/tissues by a variety of stimuli, such as heat, heme itself, heavy metals, reactive oxygen species (ROS), hypoxia, nitric oxide (NO), ultraviolet radiations, and xenobiotics. Therefore, its critical role is the cellular protection against such insults [6–8]. However, an abnormal HO-1 overexpression may be responsible for pathological conditions; for example, it can modify the endogenous balance between apoptosis and proliferation, promoting cancer formation and maintenance [9,10]. Indeed, besides healthy human cells, HO-1 is highly expressed in several solid tumors as well as hematopoietic neoplasms in which it exerts a critical role as survival molecule, being involved in their growth, metastasis, angiogenesis, and tolerance to chemo-, radio- and photodynamic therapies [11–13].

Chronic myeloid leukemia (CML) is a hematopoietic stem cell malignancy, representing about 15% of leukemias in adults. It origins from a t(9;22) chromosomal translocation that generates the BCR-ABL oncogene. The product of this oncogene is the BCR-ABL protein with very high tyrosine kinase (TK) activity, which in turn leads to an uncontrolled proliferation of myeloid stem cells with consequent initiation, maintenance and progression of CML [14]. Indeed, blockade of BCR-ABL protein with tyrosine kinase inhibitors (TKIs) is a well-validated approach for the treatment of CML

[15]. Imatinib (IM, marketed as Glivec® or Gleevec®) is the first discovered TKI approved by the FDA in 2001. From that date, it achieved great clinical success becoming the first-line drug in conventional treatment of CML [16]. Despite this smashing success, its clinical use is often associated with the emergence of clinical resistance [17,18]. To overcome IM resistance, several classes of new-generation TKIs have been developed in the last years, and some of them, such as dasatinib, nilotinib, bosutinib, and ponatinib, are currently approved drugs. Although the pharmacological use of TKIs has changed CML from a largely incurable disorder to a disease compatible with a normal lifespan, crucial issues remain to be solved, mainly the permanence of 10–15% of patients resistant to all TKIs and at risk of disease progression. Therefore, new strategies to improve CML therapy may provide additional therapeutic options for patients in this setting. The most common mechanism of IM resistance is the result of point mutations in BCR-ABL TK domain [19]. Besides gene point mutations, IM resistance may be due to amplification of the BCR-ABL gene with consequent overexpression of BCR-ABL itself [20]. This amplification imposes a continuous increase of IM dosage with consequent more severe side effects. Moreover, there are evidences that BCR-ABL protein promotes novel acquired cytogenetic aberrations of other signal pathways, such as the expression of a number of antiapoptotic proteins, among which HO-1 is one of the most representative. HO-1 is constitutively expressed in primary CML cells and its expression is higher in IM-resistant cell lines, such as K562R and LAMA-84R cells, than in IM-sensitive ones [21,22]. A recent study has provided evidence that silencing HO-1 in the mentioned cell lines, increased apoptosis and restored IM activity [23]. According to this study, we recently demonstrated that two novel imidazole-based HO-1 inhibitors **1** (LS0) and **2** (LS1/71) (Figure 1), were able to restore IM sensitivity in LAMA-84R cells producing growth-inhibitory effects [24]. Interestingly these effects were obtained only by means of a combination of IM and HO-1 inhibitors, whereas the single molecules were not effective. These studies confirmed that HO-1 over-activity is responsible for IM-resistance and that HO-1 inhibition can be a viable new anticancer strategy [10,25,26]. Co-treatment with IM and HO-1 inhibitors could find application in

chronic phase (CP)-CML patients that develop IM resistance and clinically treated with increasing doses of IM. Synergism between HO-1 inhibitors and IM might decrease IM dosage and side effects in these patients. Therapeutic application of these findings would require two molecules (IM and HO-1 inhibitor) co-administration, but combination therapy is generally a difficult and complicated avenue because it can give rise to drug-drug interactions, as well as a negative patient compliance. An alternative strategy would be to combine multiple activities within the same compound providing a superior therapeutic effect and side effect profile, compared to the action of single molecules. In this respect, conjugation of two biologically active molecules into one hybrid compound can be beneficial for the treatment of diseases with complex etiologies such as cancer [27].

On these bases, in this study we designed and synthesized a new series of hybrid compounds, namely hybrid HO-1/TKI, containing an aryloxyalkylimidazole moiety and an "IM-like portion" (**6a**–**n**, Figure 1), needed for the interaction with HO-1 and BCR-ABL proteins, respectively. In order to gain insight on the structure activity relationships (SAR), we synthesized various HO-1/TKIs with the oxybutylimidazole moiety connected at different positions of the benzamide ring and characterized by the presence of various substituents in the same phenyl ring. We tested all hybrids to evaluate their capacity of inhibiting the enzymatic activity of both targets and reducing the viability of IM-resistant and sensitive CML cells. To obtain information on the binding mode of these HO-1/TKIs towards both proteins and to explain the differences in the experimentally observed activities, we performed molecular docking studies. Finally, we investigated the mechanism of action and carried out an *in silico* prediction of ADME toxicity for the most promising compounds.

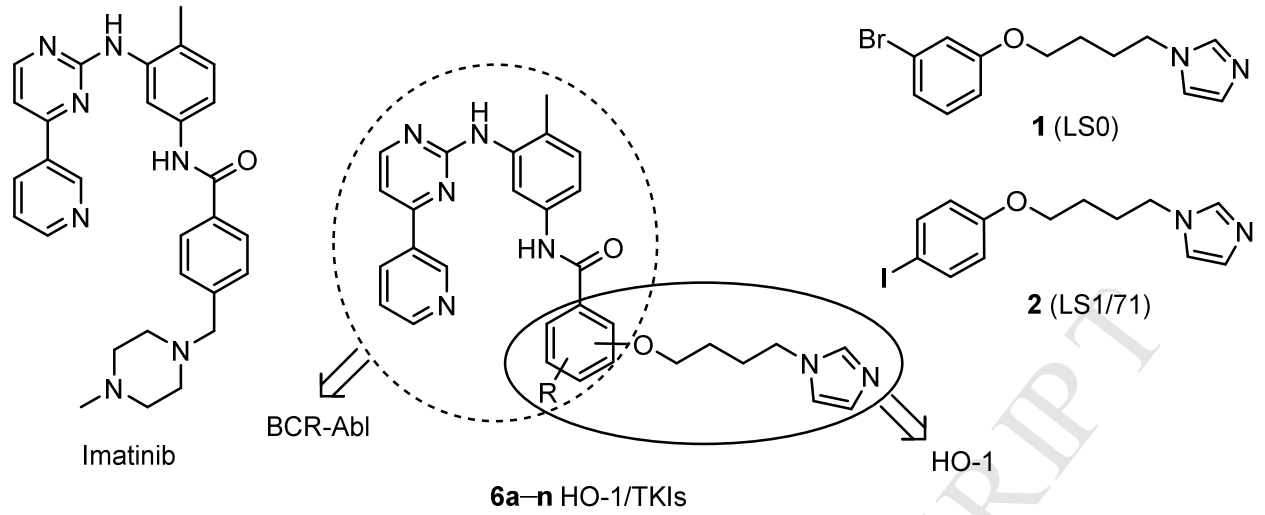

Figure 1. Chemical structures of IM and parent compounds **1** and **2**, and general structure of HO-1/TKI hybrids **6a**–**n**.

2. Results and Discussion

2.1. Chemistry

The synthesis of HO-1/TK hybrid compounds **6a**–**n** was accomplished in three steps, as outlined in Scheme 1. In the first step, the commercially available hydroxybenzoic acid methyl esters were etherified with 1,4-dibromobutane to give corresponding bromobutoxy benzoates **3a**–**n**. In the second step nucleophilic displacement of the intermediates **3a**–**n** with imidazole in acetonitrile under microwave irradiation, in the presence of triethylamine (TEA) and tetrabutylammonium bromide (TBAB), at 95 °C for 30–45 min, gave the desired methyl imidazolylbutoxy benzoates **4a**–**n**. In the final step, condensation of methyl esters **4a**–**n** with 4-methyl-N^3-[4-(pyridin-3-yl)-pyrimidin-2-yl]1,3-benzenediamine (**5)** in dry tetrahydrofuran (THF), in the presence of potassium *tert*-butoxide (*t*BuOK), at room temperature, under nitrogen, gave final hybrid compounds **6a**–**n**.

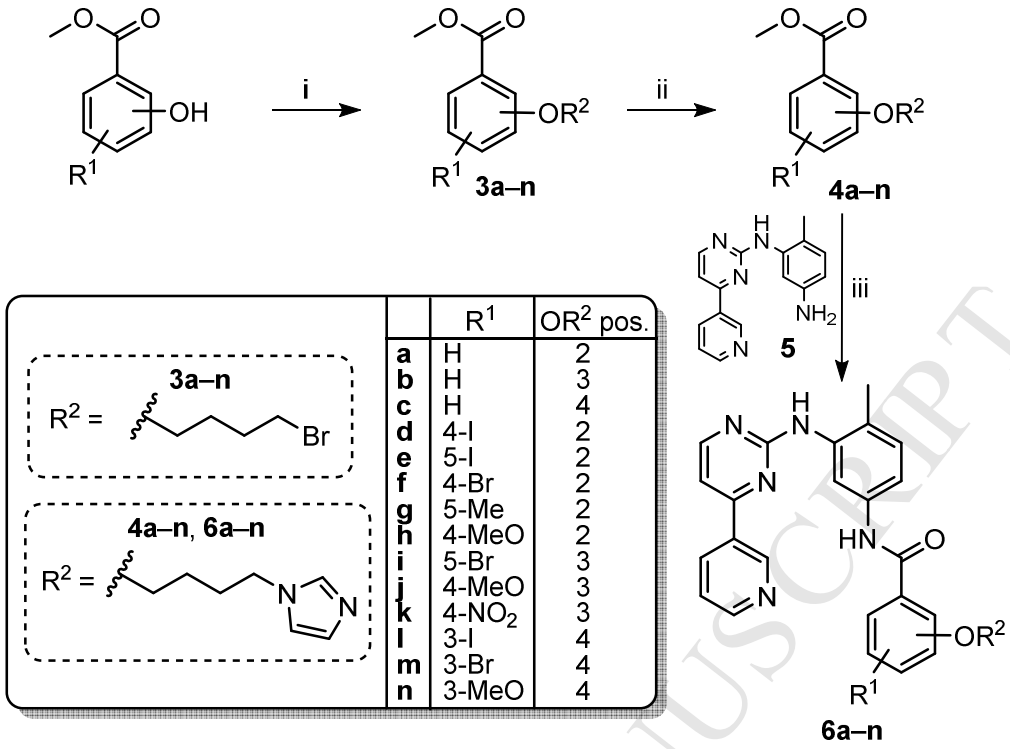

Scheme 1. Synthesis of HO-1/TKI hybrids **6a**–**n**. Reagents and conditions: (i) method A, 1,4-dibromobutane, acetone, K_2CO_3, 90 °C under microwaves irradiation; method B, 1,4-dibromobutane, dimethylsulfoxide, KOH, room temperature; method C, 1,4-dibromobutane, acetonitrile, K_2CO_3, reflux. (ii) Imidazole, acetonitrile, TEA, TBAB, 95 °C, under microwaves irradiation. (iii) intermediate **5**, dry THF, *t*BuOK, room temperature, under nitrogen.

2.2. Biological evaluation

Designed and synthesized compounds **6a**–**n** are hybrid compounds bearing the pharmacophoric portions for inhibition of HO-1 and TK, respectively. Since the structure of these hybrids is very close to that of IM, but rather different with respect to HO-1 inhibitors **1** and **2** (Figure 1), a crucial challenge was to demonstrate whether HO-1 inhibition was maintained. Thus, as a first step, we tested the ability of all compounds of inhibiting HO-1 enzymatic activity. We focused our attention towards HO-1 since only this inducible isoform is involved in tumorigenesis and in tumor progression, and is extremely overexpressed in cancer such as CML. HO-1 was obtained from the microsomal fractions of rat spleen, and its activity was determined by measuring the bilirubin

formation using the difference in absorbance at 464–530 nm, as described in the experimental section [28]. Compounds **1** and **2** (Figure 1), and azalanstat (Table 1, Figure S1, supporting information, SI) were used as reference substances. Azalanstat is the first discovered imidazole-based HO-1 inhibitor, representing the lead-compound for SAR and crystallographic studies in the field of HO-1 inhibitors [29–32]. Despite its potential hepatotoxicity at high doses, imidazole nucleus is the central core in many commercially available drugs, such as antimycotic agents, and continues to be widely used in the development of new potential pharmacologically active compounds [33–35]. One of the most critical issues in the clinical use of azole based HO-1 inhibitors is the non-selectivity towards other heme-containing enzymes, such as nitric oxide synthase, soluble guanylate cyclase, and cytochrome P450. For this reason azalanstat and some of its congeners were tested on above-mentioned hemoproteins, and showed a good profile of selectivity for HO-1 [36]. HO-1 inhibition by **6a**–**n** is expressed as IC_{50} (μM) and results are summarized in Table 1. It is evident that all hybrids inhibited HO-1 at micromolar concentrations, with IC_{50} values ranging from 0.9 to 74 μM, and in sub-micromolar range for three of them, **6f**, **6g**, and **6m**. Inhibition potency of these last compounds is comparable to or higher than those of the parent compounds **1** and **2**, and better than that of azalanstat. Additionally, compound **5** (representing the "IM-like portion" of the hybrids) as well as IM, were not active on HO-1, confirming that HO-1 inhibition is due to the imidazole portion of the molecules. SAR studies revealed that the position of the oxybutylimidazole moiety OR^2 strongly influenced HO-1 inhibition. The best results were obtained when this moiety was in the 2- position of the benzamide ring with respect to the 3- and, above all, the 4-substituted compounds (**6a** *vs* **6b** and **6c**, or **6d** and **6e** *vs* **6l**). Indeed, hybrids **6f** and **6g** were the most potent compounds in this series. The only exception to this rule was given by derivative **6m** which, despite being a 4-substituted compound, inhibited HO-1 in submicromolar concentration. Regarding the effect of the substituent R^1, generally unsubstituted compounds were less potent than those carrying a substituent; among selected substituents, bromine generally gave the best contribution (**6f**, **6i**, and **6m**). Taken together,

these results confirm that these compounds behave as imidazole-based HO-1 inhibitors, although the different chemical structure with respect to the parent compounds **1** and **2**.

Table 1. Inhibition potency of hybrids **6a**–**n** towards HO-1.

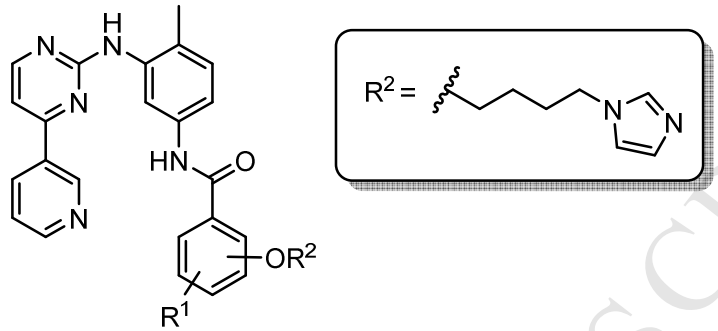

Compound	R^1	OR^2 position	HO-1 IC_{50} (μM) ± SD[a]
6a	H	2	28.02 ± 0.8
6b	H	3	38.54 ± 1.2
6c	H	4	66.23 ± 2
6d	4-I	2	15.13 ± 0.2
6e	5-I	2	38.87 ± 1.1
6f	4-Br	2	0.95 ± 0.01
6g	5-CH_3	2	0.95 ± 0.02
6h	4-OCH_3	2	61.56 ± 2.1
6i	5-Br	3	28.65 ± 1.8
6j	4-OCH_3	3	15.14 ± 0.9
6k	4-NO_2	3	4.03 ± 0.1
6l	3-I	4	74.89 ± 2.1
6m	3-Br	4	0.92 ± 0.01
6n	3-OCH_3	4	56.61 ± 2.3
5	—	—	> 100
IM	—	—	> 100
1	—	—	2.10 ± 0.3
2	—	—	1.00 ± 0.05
Azalanstat[b]	—	—	6 ± 1[c]

[a]Each value is the mean ± SD of three determinations; [b]Figure S1; [c]Value from reference [29]

Subsequently, we evaluated if compounds **6a**–**n** were able to reduce the viability of CML cells. We used both IM-resistant (K562R) and IM-sensitive (K562S) cell lines. The K562R cells were selected because they did not have the two most common mutations in BCR–ABL gene, i.e. T315I and P-binding phosphate loop (P-loop) mutations [37]. In these cells, resistance mechanism is mainly due to BCR-ABL gene amplification and HO-1 over-expression, as already experimentally

reported by Tibullo *et al.* [23]. Results, reported in Table 2, were determined by a XTT assay as described in experimental section and are expressed as IC_{50}. IM and HO-1 inhibitors **1** and **2** were used as reference compounds.

Table 2: Viability of resistant and sensitive CML cell lines in the presence of hybrid compounds **6a**–**n**. K562R and K562S were incubated for 24 h with various concentrations of compounds **6a**–**n** and cell viability was assessed using the XTT assay kit.

Compounds	IC_{50} (μM)[a]	
	K562R	**K562S**
6a	83.42 ± 2.2	47.50 ± 1.3
6b	63.40 ± 1.8	74.57 ± 2.1
6c	99.38 ± 2.3	49.89 ± 1.2
6d	51.82 ± 1.2	57.41 ± 2.2
6e	81.70 ± 1.7	66.50 ± 0.9
6f	44.58 ± 2.1	66.09 ± 0.7
6g	48.57 ± 1.4	59.48 ± 1.0
6h	46.56 ± 0.9	58.87 ± 1.3
6i	19.14 ± 0.3	6.50 ± 0.2
6j	18.74 ± 0.7	10.11 ± 0.3
6k	47.62 ± 1.1	25.02 ± 0.8
6l	52.39 ± 1.5	32.47 ± 0.4
6m	31.76 ± 0.8	12.00 ± 0.2
6n	27.10 ± 0.7	29.51 ± 1.0
1	81.70 ± 1.7	68.30 ± 0.9
2	84.38 ± 1.3	69.09 ± 0.6
IM	98.82 ± 1.8	1.00 ± 0.09
IM + 1	27.33 ± 1.2	—
IM + 2	25.56 ± 0.9	—

[a]Each value is the mean ± SD of three determinations.

With regard to resistant cells, many hybrids were more effective with respect to single molecules, IM or imidazole-based HO-1 inhibitors **1** and **2** (IC_{50} = 98, 81, 84 μM, respectively). Specifically, some hybrids were 2 to 5-fold more potent than IM (IC_{50} = 98 μM), particularly **6i**, **6j**, and **6n** (IC_{50} = 19, 18, and 27, respectively). Notably, **6i** and **6j** were slightly more effective also with respect to the IM and **1** or **2** co-administration. This result confirms that the combination of inhibitory

properties against HO-1 and BCR-ABL in the same hybrid molecule has the same effect of IM and HO-1 inhibitors co-administration [24] with the advantage of avoiding the potential side-effects of a combination therapy. Due to HO-1 over-expression in K562R cells, it is possible to affirm that the introduction of a moiety that inhibits HO-1 in the structure of IM to give hybrids **6a–n** is critical to reduce the K562R cells viability, and contributes positively in overcoming IM-resistance. However, since the most active compounds are not those with the highest inhibitory potency towards HO-1, a contribution to the antiproliferative activity may be due to the IM-portion of the molecule or to off-target effects.

On the contrary, all compounds were less active than IM in sensitive cells. This result may be related to HO-1 activity too; indeed, inhibition of HO-1 by hybrids **6a–n** does not give a positive contribution since this enzyme is not over-expressed in K562S cells [23]. Compounds **6i** and **6j** were the most active also in these cells, particularly **6i** which showed a potency close to IM (**6i** IC_{50} = 6 μM, IM IC_{50} 1 μM). Consequently, **6i** may be considered as a lead compound for further development also for the treatment of IM-sensitive cells.

Since our attention was mainly devoted to the involvement of HO-1 in the phenomena of chemoresistance, we focused our attention on K562R resistant cells and determined the inhibitory activity of compounds **6**–**n** towards BCR-ABL protein. For this purpose, we measured the amount of phosphorylated CrKL (pCrKL) by immunoblot analysis (Figure S2, SI). CrKL is a BCR-ABL substrate whose phosphorylation reflects the level of TK activity, and which is commonly used to test BCR-ABL activity *in vivo* [38]. Results are summarized in Figure 2 and are expressed as pCrKL/CrKL ratio in K562R cells treated with 10 μM of IM or 10 μM of tested compounds, compared to the control. We selected 10 μM dose since this was, on average, the concentration at which almost all hybrids were able to inhibit HO-1. IM at the concentration of 1 μM (data not shown) and 10 μM in resistant cells was not able to inhibit phosphorylation of CrkL, whereas in sensitive cells it was effective already at 1 μM (Table 2). Of interest, many hybrids, particularly **6f**,

6i, **6j**, **6k**, **6l**, **6m**, and **6n** were more effective than IM itself in inhibiting the phosphorylation of CrkL, and consequently, in reducing TK activity of BCR-ABL protein. Differently to HO-1, hybrids with the highest TK inhibitory ability carry the oxybutylimidazole moiety at the 3- or 4-position of the benzamide ring, instead of the 2-position. This is obviously due to different SARs for the two different targets. The noteworthy result is that some hybrid compounds were able to interact with both HO-1 and BCR-ABL at micromolar concentrations, confirming that it is possible to inhibit both targets with one single molecule. Simultaneous HO-1 and BCR-ABL inhibition may have therapeutic application when IM-resistance is caused by BCR-ABL gene amplification, such as in this K562R cells, with downstream overexpression of BCR-ABL and HO-1 proteins. This is particularly true in CP-CML patients clinically treated with increasing doses of IM, as they consequently suffer more severe side effects. HO-1/TK hybrids may represent an alternative to higher IM doses, especially if their action is selective towards leukemic cells.

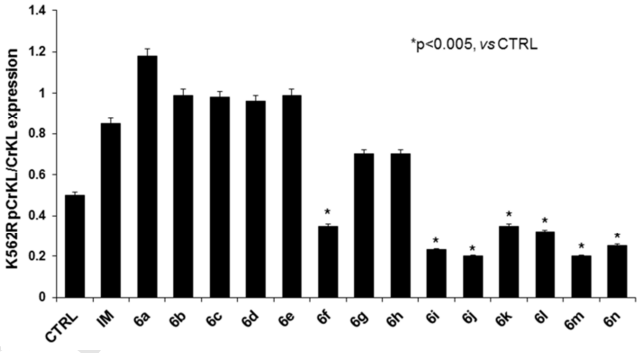

Figure 2. pCrKL expression in K562R cells treated with 10 μM IM and 10 μM hybrid compounds **6a**–**n**. Protein detection was carried out using immunoblot analysis and densitometric evaluation of protein were obtained from four experiments performed in triplicate. Data, expressed as pCrKL/CrKL ratio, represent the mean ± SD. Significant *vs* untreated control (CTRL): *p<0.005.

Lymphocytes collected from healthy volunteers were selected as an example of non-cancerous cells. The viability of these lymphocytes was tested in the presence of the most interesting

compounds (**6i**, **6j**, **6k**, **6m**, and **6n**). Since tested compounds, at 10 μM, did not alter lymphocytes viability, they can be considered non-toxic for healthy cells (Figure S17, SI).

Subsequently, we studied the mechanism of cell death. As we previously reported [24], HO-1 inhibitors **1** and **2** plus IM treatment lead to cellular apoptosis. This data, according to Datta *et al.* [39], demonstrated that down-regulation of HO-1 expression induced cellular apoptosis. In order to evaluate whether the cellular death was due to an apoptotic cell death, we determined the apoptosis profile of the most active compounds (**6i**, **6j**, **6k**, **6m**, and **6n**) using a cytofluorimetric assay. Results are shown in Figures 3 and 4. All the tested compounds were able to increase the number of apoptotic dead cells to a greater extent than IM. In particular, compounds **6i**, **6j**, and **6n** highly reduced the viability of resistant cells increasing the number of cells in late and early apoptosis. Among them, hybrids **6i** and **6j** were the most potent, then they were selected for more in-depth biological studies.

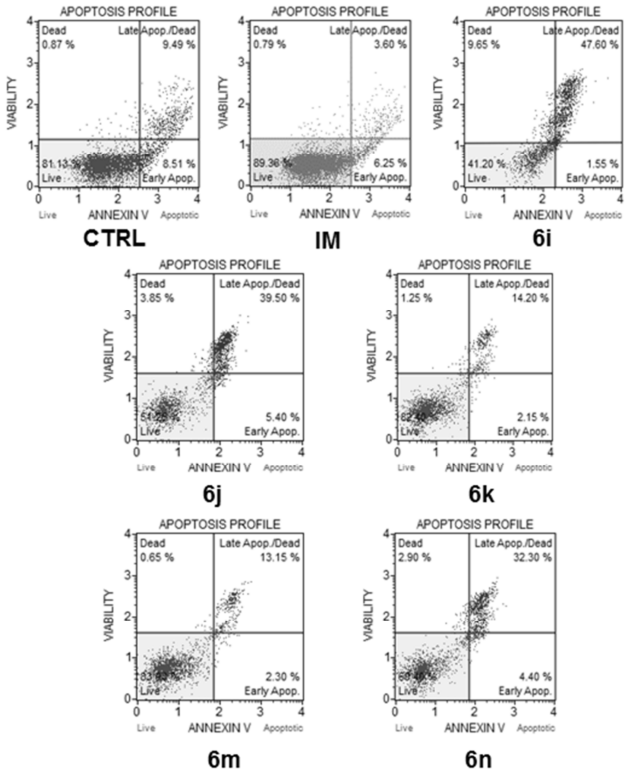

Figure 3. Representative apoptotic profile of K562R cells untreated and treated with 10 μM IM and 10 μM **6i**, **6j**, **6k**, **6m**, **6n** hybrid compounds. Each profile shows the percentage of live, apoptotic and dead cells.

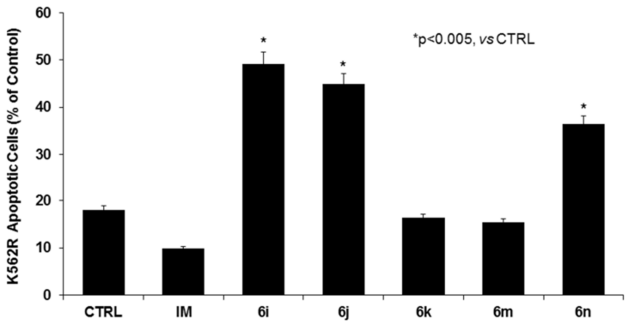

Figure 4. Percentage of apoptotic K562R cells untreated and treated with 10 μM IM and 10 μM **6i**, **6j**, **6k**, **6m**, **6n** hybrid compounds. Values represent the means ± SD of four experiments performed in triplicate. Significant *vs* untreated control (CTRL): *p<0.005.

In particular, we desired to determine whether HO-1 inhibition was maintained in intact cells too. At this purpose, we measured HO-1 enzymatic activity in K562R cells treated with 10 μM IM, **1**, **2** imidazole compounds, and 10 μM hybrids **6i** and **6j**, with respect to untreated cells. Results, described in Figure 5, show that both compounds reduced the HO-1 activity in the lysates obtained after treatment of intact cells, thus behaving as HO-1 inhibitors. Therefore, as parent compounds **1** and **2**, they are effective not only in broken-cell preparations but also in intact cells, suggesting that they are able to cross the cellular membrane and might have a potential *in vivo* application.

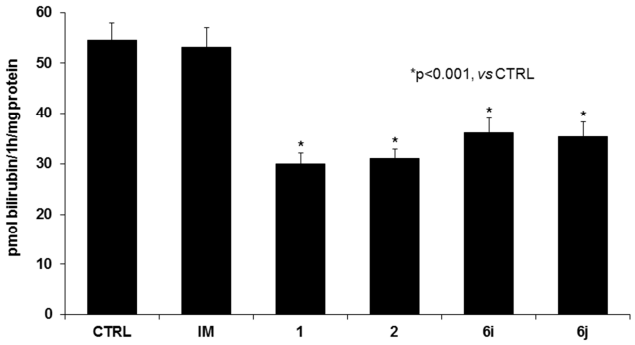

Figure 5. HO-1 activity in K562R cell lysate obtained after 24 h cell treatment in absence and in presence of 10 μM IM, **1** and **2** imidazole compounds, **6i** and **6j** hybrid compounds. HO-1 activity was determined by measuring the bilirubin formation using the difference in absorbance at 464 to 530 nm as described in the experimental section. Values represent the means ± SD of four experiments performed in triplicate. Significant *vs* untreated control cells: *p<0.001.

It is generally recognized that, in some specific cases, HO-1 inhibition may induce HO-1 expression *in vivo*, giving rise to opposite effects to the expected results. This is particularly true for metalloporphyrins (Mps), which are HO-1 inhibitors structurally related to heme and which consequently act as competitive HO-1 inhibitors [40]. HO-1 induction, together with other side-effects of Mps, limit their clinical use. Therefore, in the present paper, in order to exclude a potential indirect HO-1 induction, we measured HO-1 and HO-2 mRNA levels in K562R cells treated and untreated with IM, **1** and **2** reference compounds, and with hybrid compounds **6i** and **6j** (Figure 6). Results revealed that compounds **6i** and **6j** markedly decreased mRNA levels of HO-1, whereas HO-2 mRNA levels were not modified. In contrast, IM gave opposite effects since enhanced HO-1 mRNA expression. These results confirmed what had been observed in our previous paper about the combination of IM and the parent HO-1 inhibitors, **1** and **2** [24]. Thus, compounds **6i** and **6j**, contrarily to Mps and other HO-1 inhibitors, do not behave as HO-1 inducers but they are both able to down-regulate HO-1 expression and to inhibit HO-1 activity.

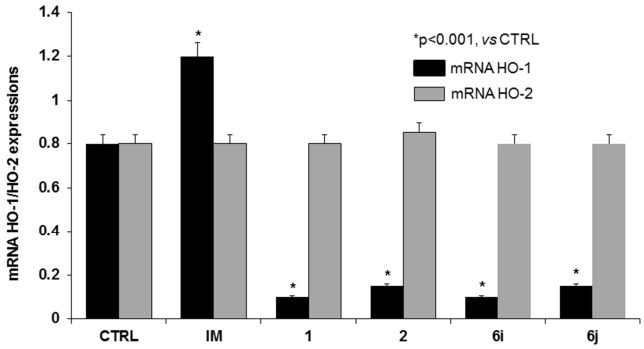

Figure 6. Effect of 10 μM IM, **1** and **2** imidazole compounds, 10 μM **6i** and 10 μM **6j** on mRNA expression analyzed by Real-Time PCR. Values represent the means ± SD of four experiments performed in triplicate. Significant *vs* untreated control cells: *p< 0.005.

Furthermore, since the apoptotic effect of IM is mediated by ROS formation in IM-sensitive cells [23], here we measured the intracellular oxidants levels in K562R cells untreated and treated with IM, **1**, **2** imidazole compounds, and with compounds **6i** and **6j**. Results in Figure 7 clearly show that IM was not effective, and treatment with compounds **1** and **2** slightly increased ROS levels. On the contrary, treatment with **6i** and **6j** give the highest effect. This effect may be related to the HO-1 down-regulation observed for compounds **6i** and **6j** (Figure 6). Specifically, low levels of HO-1 protein and HO-1 activity decrease the protection of tumor cells against oxidant species. Then compounds **6i** or **6j** treatment leads to an increase of ROS amount and of the percentage of apoptotic cells (Figure 3 and 4). Therefore, the simultaneous inhibition/down-regulation of HO-1 and inhibition of TK may increase ROS and the elevated ROS levels may facilitate tumor killing.

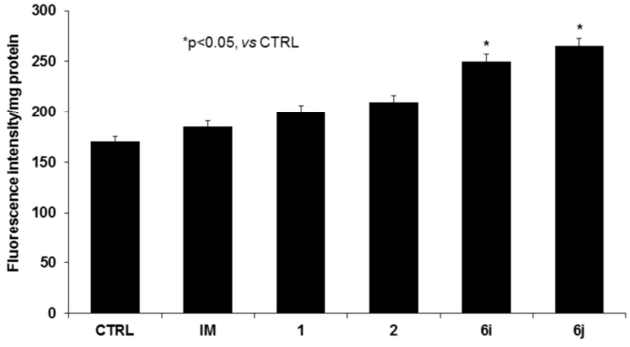

Figure 7. Intracellular oxidants in K562R cells untreated and treated with 10 μM IM, **1** and **2** imidazole compounds or 10 μM **6i** and **6j**. The fluorescence, corresponding to the oxidized radical species 2',7'-dichlorofluorescein (DCF), was spectrofluorometrically monitored (excitation, λ = 488 nm; emission, λ = 525 nm). Values, expressed as fluorescence intensity (F.I.) of oxidized radical species 2',7'-dichlorofluorescein (DCF)/mg protein, represent the means ± SD of four experiments performed in triplicate. Significant *vs* untreated control cells: *p< 0.05.

2.3. Docking studies

In order to study the interaction of the new set of compounds **6a**–**n** with HO-1 and with BCR-ABL kinase, a molecular docking study was performed. We investigated the binding modes of **6a**–**n** in comparison with (2*R*,4*S*)-2-[2-(4-chlorophenyl)ethyl]-2-[(1H-imidazol-1-yl)methyl]-4-[((5-trifluoromethylpyridin-2-yl)thio)methyl]-1,3-dioxolane (QC-80, Table 3, Figure S1, SI) in HO-1 and IM in BCR-ABL kinase. The X-ray crystal structures of the co-crystal HO-1/QC-80 (PDB code 3HOK) [30] and of the crystal structure of the BCR-ABL kinase domain in complex with IM (PDB code 1IEP) [41] were used as the protein structures. Docking was performed using AutoDock [42]. To validate the docking model, we docked molecules QC-80 and IM to the original binding sites of the respective proteins, to compare their experimental and calculated binding potencies. Particularly, we used the same validated docking procedure as previously published by our research group for the validation of the HO-1 model [43–45]. On the other hand, for the validation of the BCR-ABL kinase model, we compared our results with the ones of Lin et al [46]. Results reported in Tables 3 and 4 showed that our calculated binding potencies are in good agreement with the experimental ones [30,47], and that the simulated complexes of QC-80 and IM show high correspondence to the corresponding crystallographic structure with a RMSD value of 0.75 Å and 0.76 Å respectively. Once validated the model, two different set of molecules, representative of the different potencies at the two different proteins, were chosen: **6a**, **6f**, **6g**, **6j**, **6l**, and **6m** were used in the docking experiment for HO-1 whereas **6a**, **6g**, **6i**, **6j**, and **6l** were docked into the binding site of

BCR-ABL kinase. For molecules **6l** and **6m**, best binding energies for HO-1 were obtained after a molecular dynamics simulation. The docked poses and the 2D-interaction inside HO-1 and BCR-ABL are shown in Figures 8 and 9, and in Figures S3–S15 in the SI.

The results of the docking calculation and the docking poses for HO-1 are reported in Table 3 and in Figures 8 and S3–S9 (SI), respectively. The calculated binding potencies are in good agreement with the experimental values in the HO-1 inhibition assay, as it is possible to see from a comparison between the calculated K_i and the experimental IC_{50} (Figure S16 A). In all of the docked compounds, the iron(II) of the heme in HO-1 is correctly coordinated by the nitrogen atom of the imidazole ring of the studied compounds in the eastern pocket. By means of this coordination binding, iron(II) is protected from oxidation by disruption of an ordered solvent structure involving the critical Asp140 hydrogen-bond network (Tyr58, Tyr114, Arg136, and Asn210) and consequent displacement of water residues needed for catalysis. On the other hand, the position of the oxylbutylimidazole (OR^2) and the R^1 group greatly influence the potency and the dual activity of molecules. Looking at the poses of the docked compounds (Figure 8, left), we can see that when the oxylbutylimidazole group is in 2 position, the molecules (**6a**, **6f**, and **6g**) form a series of interactions with the internal hydrophobic pocket of the protein (Figure 8, right), particularly in the western region [30], and the flexible linker capped with imidazole points to the heme group, making possible the important interaction with the iron(II). On the other hand, when the oxylbutylimidazole group is in 4 position (**6l** and **6m**), the same interactions are not allowed due to steric hindrance in the positioning of the molecules inside the internal pockets. However, the potent compound **6m** performs stabilizing interactions on the surface of the protein. In particular, the bromine atom is easily located into a pocket formed by Phe37, Leu147 and Ile150 and a hydrogen bond is formed with Gln38. In the case of the less potent compound **6l**, its bigger iodine atom cannot be located inside the same pocket and the molecule, flipping itself, does not get this set of interactions, that are the probable cause of the potency of the bromine derivative. When the oxylbutylimidazole group is in 3-position (**6j**), the "IM-like portion" of the molecule is pushed to the external portion of the

western pocket, but the major part of the molecule is still inside the pocket. Regards the R^1 substituent, small substituents are easily tolerated and can increase the activity when they are localized in 4- or 5-position and the oxylbutylimidazole group is in 2-position. Particularly, these substituents are located into an internal hydrophobic pocket; for example, in molecules **6f** and **6g**, two of the most active compounds, the methyl and the bromine group are easily accommodated in a pocket formed by Val50, Arg136, Phe166 and Ser14, and in the case of compound **6f**, the bromine atom can interact through a halogen bond interaction with Asn210.

Table 3. Docking results for the studied molecules in 3HOK.

Compound	IC_{50} (μM)	ΔG_B (kcal/mol)	Calc. K_i (μM)
QC-80[a]	2.1[b]	–7.55	2.9
6a	28	–6.39	20.59
6f	0.95	–7.89	1.63
6g	0.95	–8.50	0.58
6j	15	–6.70	12.2
6l	74	–5.89	47.9
6m	0.9	–7.58	2.76

[a]Figure S1; [b]Value from reference [30]

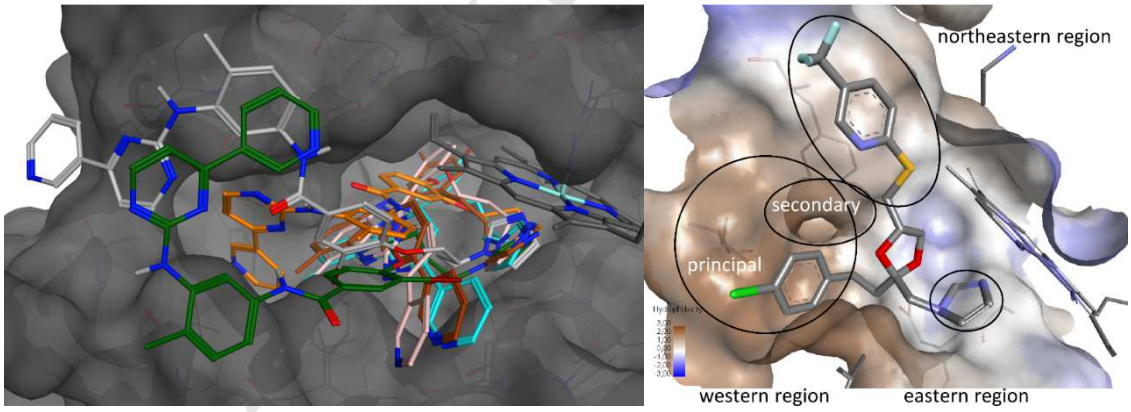

Figure 8. Left: Docked poses inside HO-1 (3HOK) of: **6a** (light pink), **6f** (light blue), **6g** (dark orange), **6j** (light orange), **6l** (dark green), and **6m** (light gray). Right: Binding regions of the hydrophobic pocket inside the HO-1 with the QC-80 ligand (PDB ID: 3HOK).

Regarding the activity towards BCR-ABL, the calculated binding energies and the poses of the studied compounds are shown in Table 4 and in Figures 9 and S10–S15 (SI), respectively. All the studied molecules are able to interact with the protein in a similar way to that of reference compound IM. Results of calculated binding energies showed in Table 4 point out the high correlation between the estimated free energies of binding and percentage of inhibitory efficiency values of our compounds. Particularly, compounds **6i**, **6j**, and **6l** resulted better than IM in reducing TK activity (Figure 9), rather than compounds **6a** and **6g** that possess a lower activity than IM (Figure S16 B). The *N*-(4-methyl-3-((4-(pyridin-3-yl)pyrimidin-2-yl)amino)phenyl) moiety is always located in the same pocket formed by Ile313, Tyr253, Leu248, Phe317, Met318, Leu370, Val256 and Thr315. Conversely, the oxylbutylimidazole group is pointing to the external surface of the protein in all docked compounds and can be oriented in different ways in relation to the position of insertion on the benzamide ring. Judging by the docking results, and looking at the biological results, we can conclude that the oxylbutylimidazole moiety can be positioned in 2, 3 and 4 position without any influence in the positioning of the central core of the "IM-like portion" of the molecule, that in all case can interact in the right way with the protein. Nevertheless, some important differences can be obtained with the R^1 substituents. For example, the methyl group in 5-position of **6g** decreases the activity of the molecule for a steric clash with Leu298 and Ile293, whereas the bromine in 5-position of **6i** is well accommodated in a near pocket formed by Leu354, Ile293, Val289 and Phe359 [48].

Table 4. Docking results for the studied molecules in 1IEP

Compound	ΔG_B (kcal/mol)	Calc. K_i (μM)
IM	–8.99	0.25
6a	–7.15	5.70
6g	–7.93	1.53
6i	–10.87	0.01
6j	–10.67	0.01
6l	–10.21	0.03

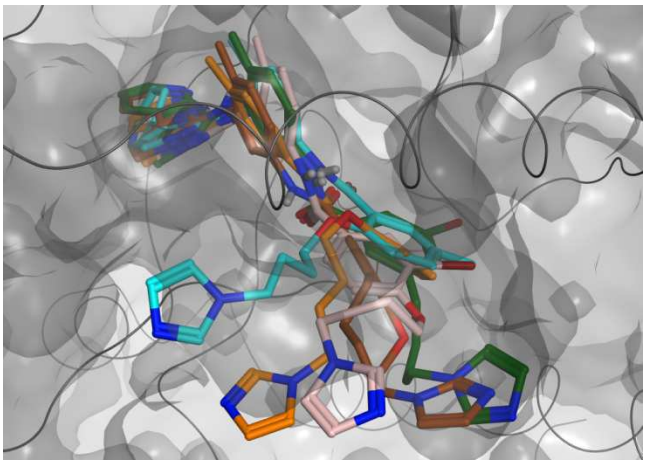

Figure 9. Docked poses inside BCR-ABL (1IEP) of: **6a** (light orange), **6g** (light blue), **6i** (dark green), **6j** (dark orange), and **6l** (light pink).

2.4. ADME and toxicity risk assessment

To evaluate if the designed compounds could display a good pharmacokinetic profile and no adverse side effects (ADME-Toxicity), we conducted an *in silico* study for the two selected compounds **6i** and **6j**. The results are reported in Tables 5 and 6. The *in silico* ADME results (Table 5) clearly show that compounds **6i** and **6j** should exhibit a good oral availability (human intestinal absorption, HIA >95%) and a discrete Caco-2 cell permeability (35.36 nm s^{-1} for **6i** and 48.10 nm s^{-1} for **6j**) but with a strong plasma protein binding (PPB >95%). Interestingly, both compounds **6i** and **6j** are predicted to barely permeate the blood-brain barrier with an *in vivo* BBB penetration (C_{brain}/C_{blood}) of 0.05 and 0.11, respectively. Moreover, our new molecules resulted non-mutagen, non-tumorigenic, non-irritant and without negative effects on the reproductive system (Table 6). Finally, of the two compounds, only **6j** has a positive value of drug-likeness, establishing that the molecule predominantly contains common fragments that are present in commercial drugs; both compounds have a positive value of drug-score, encompassing the contributions of partition coefficient, solubility, molecular weight, drug-likeness and the four toxicity risks.

Table 5. Selected *in silico* ADME profiling for molecules **6i** and **6j**.[a]

Compound	Absorption		Distribution	
	HIA (%)	*In vitro* Caco-2 cell permeability (nm s^{-1})	*In vitro* PPB (%)	*In vivo* BBB penetration (C_{brain}/C_{blood})
6i	96.90	35.36	100.00	0.05
6j	95.79	48.10	95.88	0.11

[a]The properties related to ADME were predicted using PreADMET web-based application (http://preadmet.bmdrc.kr).

Table 6. *In silico* toxicity parameters for molecules **6i** and **6j**.[a]

Compound	Mutagenic	Tumorigenic	Reproductive Effects	Irritant	Drug-Likeness	Drug-Score
6i	none	none	none	none	–1.51	0.16
6j	none	none	none	none	0.34	0.30

[a]The properties related to toxicity were predicted using DataWarrior software [49].

3. Conclusion

In conclusion, in the present study, we discovered novel HO-1/TKI hybrid compounds **6a**–**n** able to inhibit both the enzymatic activity of HO-1 and BCR-ABL. The new compounds target simultaneously the pathway responsible for the development of CML disease and one of the pathways accountable for the onset of IM-resistance. To the best of our knowledge, it is the first time that the structure of a HO-1 inhibitor was combined into a hybrid compound. Binding mode of these hybrids with HO-1 is very similar to that observed for azole-based HO-1 inhibitors described so far. Specifically, the position of the oxybutylimidazole moiety is critical for HO-1 interaction, since 2-substituted compounds show better poses within the HO-1 protein, according to experimental values of HO-1 inhibition. Also interactions to BCR-ABL protein are similar to those observed for the reference compound IM. Many of these hybrids reduce cell viability of CML resistant cells to a greater extend with respect to IM. The most interesting compounds **6i** and **6j** enhanced cellular death by an apoptotic mechanism and by an increase of the ROS levels, and are able to cross cellular membrane since they inhibit HO-1 also in intact cells. In addition, they are able to reduce mRNA HO-1 expression, differently to Mps based HO-1 inhibitors. These results confirm that HO-1 inhibition may help to overcome resistance in CML and suggest further application of HO-1 inhibitors in other cancers in which HO-1 overexpression is involved [50].

Further studies, supported by the good predicted values of drug-score observed for **6i** and **6j**, may be designed to validate the potential clinical application of such hybrid compounds to overcome IM-resistance *in vivo*.

4. Experimental section

4.1. Chemistry

4.1.1. General details

Melting points were determined in an Electrothermal IA9200 apparatus with a digital thermometer in glass capillary tubes. Elemental analyses for C, H, N, S were within ± 0.4% of theoretical values and were performed on a Carlo Erba Elemental Analyzer Mod. 1108 apparatus. The IR spectra were recorded in KBr disks or Neat, on a Perkin Elmer 1600 series FT-IR spectrometer. ^{1}H NMR spectra were determined with Varian Inova Unity (200 MHz) spectrometer and ^{13}C NMR spectra were determined with Varian Inova Unity (500 MHz) spectrometer in DMSO-d_6 solution. Chemical shifts are in δ values (ppm) using tetramethylsilane and DMSO as the internal standard for ^{1}H NMR and ^{13}C NMR spectra, respectively; coupling constants (*J*) are given in Hz. Signal multiplicities are characterized as s (singlet), d (doublet), t (triplet), q (quartet), m (multiplet), br (broad signal). ESI-HRMS were determined with a Thermo Fischer Scientific LTQ Orbitrap XL. Reactions were monitored by thin-layer chromatography (TLC) on Merck plates (Kieselgel 60 F_{254}) and spots were visualized under the UV light (λ = 254 and 366 nm) or in an iodine chamber. The purity of all final compounds was 95% or higher. Preparative column chromatography was performed using Merck silica-gel 60 (230–400 mesh) or Biotage® SNAP cartridge KP-Sil. Microwave irradiation experiments were carried out with a CEM Discover instrument using closed Pyrex glass tubes (ca. 10 mL) with Teflon-coated septa. All chemicals and solvents were reagent grade and were purchased from commercial sources.

*4.1.2. General procedure for the synthesis of OH-1/TKI hybrid final compounds **6a–n**.*

A solution of methyl imidazolylbutoxybenzoates **4a**–**n** (1 mmol) and **5** (0.8 mmol) in 10 mL of anhydrous THF, was added with *t*BuOK (6 mmol) under nitrogen atmosphere. The reaction mixture was stirred at room temperature for 1/2 h, quenched by adding brine, and extracted by ethyl acetate (3 × 70 mL). The combined extracts were washed with water, dried on anhydrous sodium sulfate, and evaporated to obtain a residue which was purified by flash column chromatography on silica gel using mixtures of ethyl acetate/methanol as eluent.

*4.1.2.1. 2-[4-(1H-Imidazol-1-yl)butoxy]-N-[4-methyl-3-[[4-(pyridin-3-yl)pyrimidin-2-yl]amino]phenyl]benzamide (**6a**).*

Pale yellow solid; mp 85.5–86.1 °C; yield 30%. IR (KBr) cm^{-1} 3566, 3351, 2942, 1654, 1578, 1558, 1450, 1418, 1294. ^{1}H NMR (DMSO-d_6) δ 10.09 (s, 1H), 9.28 (d, J = 1.6 Hz, 1H), 9.04 (s, 1H), 8.69 (dd, J = 4.6, 1.4 Hz, 1H), 8.52–8.44 (m, 2H), 8.07 (d, J = 1.6 Hz, 1H), 7.64 (dd, J = 7.6, 1.6 Hz, 1H), 7.54–7.42 (m, 4H), 7.34 (dd, J = 8.0, 1.8 Hz, 1H), 7.21-7.02 (m, 4H), 6.81 (br s, 1H), 4.10 (t, J = 6.2 Hz, 2H), 3.94 (t, J = 6.6 Hz, 2H), 2.22 (s, 3H), 1.88–1.64 (m, 4H). ^{13}C NMR (DMSO-d_6) δ 164.16, 161.57, 161.10, 159.39, 155.75, 151.32, 148.15, 137.91, 137.08, 137.01, 134.35, 132.17, 131.86, 130.18, 129.70, 128.29, 127.40, 125.15, 123.72, 120.52, 119.00, 116.14, 115.72, 112.88, 107.52, 67.69, 45.44, 27.18, 25.59, 17.63. Anal. Calcd. for $C_{30}H_{29}N_7O_2$: C, 69.35; H, 5.63; N, 18.87. Found: C, 69.04; H, 5.78; N, 18.99. HRMS (ESI) m/z $(M+H)^+$ calcd. for $C_{30}H_{30}N_7O_2^+$: 520.2461; found: 520.2459.

*4.1.2.2. 3-[4-(1H-Imidazol-1-yl)butoxy]-N-[4-methyl-3-[[4-(pyridin-3-yl)pyrimidin-2-yl]amino]phenyl]benzamide (**6b**).*

Yellow solid; mp 85.6–86.3 °C; yield 30%. IR (KBr) cm^{-1} 3568, 3274, 2942, 1653, 1581, 1557, 1448, 1417, 1289.^{1}H NMR (DMSO-d_6) δ 10.18 (s, 1H), 9.28 (d, J = 1.8 Hz, 1H), 9.01 (s, 1H), 8.68 (dd, J = 4.6, 1.4 Hz, 1H), 8.53–8.45 (m, 12H), 8.08 (dd, J = 2.0 Hz, 1H), 7.65 (s, 1H), 7.55–7.38 (m, 6H), 7.23–7.11 (m, 3H), 6.89 (s, 1H), 4.07–4.00 (m, 4H), 2.22 (s, 3H), 1.92-1.81 (m, 2H), 1.73-

1.63 (m, 2H). ^{13}C NMR (DMSO-d_6) δ 164.99, 161.55, 161.1, 159.42, 158.41, 151.32, 148.1, 137.75, 137.20, 137.03, 136.40, 134.35, 132.16, 129.97, 129.47, 128.34, 127.61, 123.72, 119.80, 119.19, 117.51, 117.22, 116.75, 113.45, 107.48, 67.09, 45.58, 27.34, 25.70, 17.60. Anal. Calcd. for $C_{30}H_{29}N_7O_2$: C, 69.35; H, 5.63; N, 18.87. Found: C, 69.19; H, 5.88; N, 19.12. HRMS (ESI) *m*/*z* $(M+H)^+$ calcd. for $C_{30}H_{30}N_7O_2^+$: 520.2461; found: 520.2458.

*4.1.2.3. 4-[4-(1H-Imidazol-1-yl)butoxy]-N-[4-methyl-3-[[4-(pyridin-3-yl)pyrimidin-2-yl]amino]phenyl]benzamide (**6c**).*

Pale yellow solid; mp 150.5–151.4 °C; yield 23%. IR (KBr) cm^{-1} 3499, 3262, 2924, 1658, 1605, 1580, 1504, 1449, 1247. ^{1}H NMR (DMSO-d_6) δ 10.06 (s, 1H), 9.28 (d, *J* = 1.6 Hz, 1H), 9.00 (s, 1H), 8.69 (dd, *J* = 4.6, 1.4 Hz, 1H), 8.52-8.45 (m, 2H), 8.07 (d, *J* = 1.8 Hz, 1H), 7.97–7.93 (m, 2H), 7.65 (br s, 1H), 7.55–7.42 (m, 3H), 7.21–7.17 (m, 2H), 7.06–7.01 (m, 2H), 6.90 (br s, 1H), 4.07–4.00 (m, 4H), 2.22 (s, 3H), 1.91–1.87 (m, 2H), 1.84–1.63 (m, 2H). ^{13}C NMR (DMSO-d_6) δ 164.65, 161.56, 161.16, 161.08, 159.42, 151.33, 148.15, 137.71, 137.30, 137.20, 134.37, 132.18, 129.93, 129.48, 128.36, 127.36, 126.98, 123.73, 119.19, 117.20, 116.71, 113.98, 107.44, 67.15, 45.57, 27.27, 25.63, 17.59. Anal. Calcd. for $C_{30}H_{29}N_7O_2$: C, 69.35; H, 5.63; N, 18.87. Found: C, 69.09; H, 5.85; N, 19.15.

HRMS (ESI) *m*/*z* $(M+H)^+$ calcd. for $C_{30}H_{30}N_7O_2^+$: 520.2461; found: 520.2457.

*4.1.2.4. 2-[4-(1H-Imidazol-1-yl)butoxy]-4-iodo-N-[4-methyl-3-[[4-(pyridin-3-yl)pyrimidin-2-yl]amino]phenyl]benzamide (**6d**).*

Pale yellow solid; mp 168.0–169.4 °C; yield 40%. IR (KBr) cm^{-1} 3587, 3343, 2944, 1648, 1600, 1580, 1533, 1443, 1414. ^{1}H NMR (DMSO-d_6) δ 10.06 (s, 1H), 9.27 (d, *J* = 1.6 Hz, 1H), 9.04 (s, 1H), 8.68 (dd, *J* = 4.8, 1.6 Hz, 1H), 8.51–8.44 (m, 2H), 8.04 (d, *J* = 1.8 Hz, 1H), 7.54–7.29 (m, 7H), 7.20–7.16 (m, 1H), 7.02 (s, 1H), 6.81 (s, 1H), 4.11 (t, *J* = 5.8 Hz, 2H), 3.94 (t, *J* = 6.8 Hz, 2H), 2.22 (s, 3H), 1.85-1.64 (m, 4H). ^{13}C NMR (DMSO-d_6) δ 163.57, 161.56, 161.07, 159.38, 156.12, 151.32,

148.13, 137.92, 137.08, 136.83, 135.34, 132.15, 131.14, 130.20, 129.48, 128.28, 127.50, 124.98, 123.72, 121.58, 119.00, 116.11, 115.69, 107.54, 98.10, 68.09, 45.32 27.05, 25.43, 17.63. Anal. Calcd. for $C_{30}H_{28}IN_7O_2$: C, 55.82; H, 4.37; N, 15.19. Found: C, 56.13; H, 4.15; N, 15.30. HRMS (ESI) *m*/*z* $(M+H)^+$ calcd. for $C_{30}H_{29}IN_7O_2^+$: 646.1427; found: 646.1425.

*4.1.2.5. 2-[4-(1H-Imidazol-1-yl)butoxy]-5-iodo-N-[4-methyl-3-[[4-(pyridin-3-yl)pyrimidin-2-yl]amino]phenyl]benzamide (**6e**).*

Yellow-orange solid; mp 159.1–162.4 °C; yield 23%. IR (KBr) cm^{-1} 3413, 3356, 2925, 1647, 1604, 1578, 1531, 1452, 1417. ^{1}H NMR (DMSO-d_6) δ 10.11 (s, 1H), 9.27 (d, *J* = 1.8 Hz, 1H), 9.03 (s, 1H), 8.68 (dd, *J* = 4.8, 1.6 Hz, 1H), 8.51–8.42 (m, 2H), 8.03 (d, *J* = 1.8 Hz, 1H), 7.83 (d, *J* = 2.2 Hz, 1H), 7.76 (dd, *J* = 8.6, 2.2 Hz, 1H), 7.54–7.42 (m, 3H), 7.32 (dd, *J* = 8.0, 1.8 Hz, 1H), 7.18 (d, *J* = 8.4 Hz, 1H), 7.01–6.96 (m, 2H), 6.80 (br s, 1H), 4.06 (t, *J* = 6.0 Hz, 2H), 3.92 (t, *J* = 6.8 Hz, 2H), 2.21 (s, 3H), 1.84–1.60 (m, 4H).). ^{13}C NMR (DMSO-d_6) δ 162.79, 161.57, 161.08, 159.41, 155.58, 151.34, 148.17, 139.89, 137.92, 137.35, 137.07, 136.78, 134.35, 132.16, 130.20, 128.27, 127.95, 127.61, 123.73, 119.01, 116.22, 115.73, 107.56, 82.94, 67.95, 45.43, 40.09, 27.10, 25.44, 17.64. Anal. Calcd. for $C_{30}H_{28}IN_7O_2$: C, 55.82; H, 4.37; N, 15.19. Found: C, 55.51; H, 4.66; N, 15.37. HRMS (ESI) *m*/*z* $(M+H)^+$ calcd. for $C_{30}H_{29}IN_7O_2^+$: 646.1427; found: 646.1426.

*4.1.2.6. 4-Bromo-2-[4-(1H-imidazol-1-yl)butoxy]-N-[4-methyl-3-[[4-(pyridin-3-yl)pyrimidin-2-yl]amino]phenyl]benzamide (**6f**).*

Yellow solid; mp 177.4–179.5 °C; yield 33%. IR (KBr) cm^{-1} 3425, 3348, 2953, 1662, 1604, 1582, 1526, 1452, 1413, 1233. ^{1}H NMR (DMSO-d_6) δ 10.06 (s, 1H), 9.27 (d, *J* = 2.2 Hz, 1H), 9.03 (s, 1H), 8.68 (dd, *J* = 4.8, 1.4 Hz, 1H), 8.51–8.41 (m, 2H), 8.04 (d, *J* = 1.6 Hz, 1H), 7.57–7.16 (m, 8H), 7.02 (s, 1H), 6.81 (s, 1H), 4.12 (t, *J* = 6.2 Hz, 2H), 3.93 (t, *J* = 7.0 Hz, 2H), 2.21 (s, 3H), 1.85–1.62 (m, 4H). ^{13}C NMR (DMSO-d_6) δ 163.41, 161.58, 161.09, 159.40, 156.50, 151.34, 148.15, 137.94, 136.83, 134.36, 132.17, 131.20, 130.22, 128.30, 127.55, 124.66, 124.54, 123.74, 123.45, 119.03,

116.14, 115.98, 115.73, 107.56, 68.20, 45.34, 27.07, 25.39, 17.64. Anal. Calcd. for $C_{30}H_{28}BrN_7O_2$: C, 60.21; H, 4.72; N, 16.38. Found: C, 60.48; H, 4.49; N, 16.61. HRMS (ESI) *m*/*z* $(M+H)^+$ calcd. for $C_{30}H_{29}BrN_7O_2^+$: 598.1566; found: 598.1561.

*4.1.2.7. 2-[4-(1H-Imidazol-1-yl)butoxy]-5-methyl-N-[4-methyl-3-[[4-(pyridin-3-yl)pyrimidin-2-yl]amino]phenyl]benzamide (**6g**).*

Yellow-orange solid; mp 65.5–67.9 °C; yield 28%. IR (KBr) cm^{-1} 3445, 3349, 2944, 1662, 1578, 1557, 1448, 1418, 1236, 802. ^{1}H NMR (DMSO-d_6) δ 10.06 (s, 1H), 9.27 (br s, 1H), 9.04 (s, 1H), 8.69–8.67 (m, 1H), 8.51–8.04 (m, 2H), 8.04 (br s, 1H), 7.56–7.16 (m, 7H), 7.05–7.01 (m, 2H), 6.83 (br s, 1H), 4.09–3.91 (m, 4H), 2.28 (s, 3H), 2.21 (s, 3H), 1.87–1.66 (m, 4H). ^{13}C NMR (DMSO-d_6) δ 164.15, 161.59, 161.11, 159.41, 153.74, 151.34, 148.15, 137.91, 137.07, 137.00, 134.36, 132.23, 132.19, 130.20, 130.03, 129.42, 128.19, 127.43, 124.66, 123.75, 119.07, 116.19, 115.77, 113.03, 107.54, 67.88, 45.50, 27.19, 25.64, 19.92, 17.64. Anal. Calcd. for $C_{31}H_{31}N_7O_2$: C, 69.77; H, 5.86; N, 18.37. Found: C, 69.45; H, 5.99; N, 18.67. HRMS (ESI) *m*/*z* $(M+H)^+$ calcd. for $C_{31}H_{32}N_7O_2^+$: 534.2617; found: 534.2615.

*4.1.2.8. 2-[4-(1H-Imidazol-1-yl)butoxy]-4-methoxy-N-[4-methyl-3-[[4-(pyridin-3-yl)pyrimidin-2-yl]amino]phenyl]benzamide (**6h**).*

Yellow-orange solid; mp 164.7–165.5 °C; yield 41%. IR (KBr) cm^{-1} 3436, 3355, 2944, 1662, 1602, 1581, 1525, 1455, 1412, 1249. ^{1}H NMR (DMSO-d_6) δ 9.91 (s, 1H), 9.28 (d, J = 1.4 Hz, 1H), 9.04 (s, 1H), 8.69 (dd, J = 4.8, 1.4 Hz, 1H), 8.52–8.46 (m, 2H), 8.05 (br s, 1H), 7.75 (d, J = 9.2 Hz, 1H), 7.56–7.43 (m, 3H), 7.33–7,28 (m, 1H), 7.19 (d, J = 8.2 Hz, 1H),7.05 (br s, 1H), 6.80 (br s, 1H), 6.68–6.65 (m, 2H), 4.14 (t, J = 5.6 Hz, 2H), 4.00 (t, J = 6.6 Hz, 2H), 3.82 (s, 3H), 2.22 (s, 3H), 1.85–1.73 (m, 4H). ^{13}C NMR (DMSO-d_6) δ 163.24, 162.78, 161.58, 161.10, 159.41, 157.51, 151.34, 148.14, 137.96, 136.97, 134.37, 132.18, 131.92, 130.25, 128.33, 127.22, 123.74, 119.05, 116.29, 116.04, 115.65, 107.55, 105.90, 99.33, 68.02, 55.54, 45.42, 27.18, 25.55, 17.62. Anal.

Calcd. for $C_{31}H_{31}N_7O_3$: C, 67.74; H, 5.69; N, 17.84. Found: C, 67.44; H, 5.88; N, 18.03. HRMS (ESI) *m*/*z* $(M+H)^+$ calcd. for $C_{31}H_{32}N_7O_3^+$: 550.2567; found: 550.2564.

*4.1.2.9. 5-Bromo-3-[4-(1H-imidazol-1-yl)butoxy]-N-[4-methyl-3-[[4-(pyridin-3-yl)pyrimidin-2-yl]amino]phenyl]benzamide (**6i**).*

Yellow solid; mp 142.0–157.8 °C; yield 45%. IR (KBr) cm^{-1} 3446, 3301, 2932, 1648, 1583, 1527, 1438, 1400, 1284, 799. ^{1}H NMR (DMSO-d_6) δ 10.26 (s, 1H), 9.28 (d, J = 1.6 Hz, 1H), 9.00 (s, 1H), 8.68 (dd, J = 4.8, 1.6 Hz, 1H), 8.53–8.44 (m, 2H), 8.06 (d, J = 2.0 Hz, 1H), 7.70–7.64 (m, 2H), 7.55–7.43 (m, 4H), 7.37–7,35 (m, 1H), 7.23–7.19 (m, 2H), 6.80 (br s, 1H), 4.11–3.97 (m, 4H), 2.22 (s, 3H), 1.90–1.79 (m, 2H), 1.72–1.62 (m, 2H). ^{13}C NMR (DMSO-d_6) δ 163.44, 161.57, 161.11, 159.44, 159.36, 151.34, 148.17, 137.85, 137.80, 137.21, 136.74, 134.37, 132.15, 130.04, 128.34, 127.87, 123.73, 122.38, 122.10, 119.98, 119.20, 117.23, 116.77, 113.34, 107.54, 67.68, 45.50, 27.21, 25.52, 17.62. Anal. Calcd. for $C_{30}H_{28}BrN_7O_2$: C, 60.21; H, 4.72; N, 16.38. Found: C, 60.53; H, 4.47; N, 16.59. HRMS (ESI) *m*/*z* $(M+H)^+$ calcd. for $C_{30}H_{29}BrN_7O_2^+$: 598.1566; found: 598.1563.

*4.1.2.10. 3-[4-(1H-Imidazol-1-yl)butoxy]-4-methoxy-N-[4-methyl-3-[[4-(pyridin-3-yl)pyrimidin-2-yl]amino]phenyl]benzamide (**6j**).*

Pale yellow solid; mp 168.0–169.7 °C; yield 38%. IR (KBr) cm^{-1} 3566, 3359, 3100, 2962, 1647, 1585, 1557, 1515, 1418, 1269. ^{1}H NMR (DMSO-d_6) δ 10.04 (s, 1H), 9.28 (d, J = 2.0 Hz, 1H), 8.99 (s, 1H), 8.68 (dd, J = 4.8, 1.6 Hz, 1H), 8.52–8.46 (m, 2H), 8.05 (d, J = 1.8 Hz, 1H), 7.66–7.42 (m, 6H), 7.22–7.18 (m, 2H), 7.06 (d, J = 8.4 Hz, 1H), 6.89 (br s, 1H), 4.08–4.01 (m, 4H), 3.84 (s, 3H), 2.22 (s, 3H), 1.90–1.80 (m, 2H), 1.70–1.63 (m, 2H). ^{13}C NMR (DMSO-d_6) δ 164.67, 161.56, 161.16, 159.42, 151.33, 150.75, 148.38, 148.16, 137.73, 137.22, 134.36, 132.17, 129.94, 128.35, 127.39, 127.11, 123.72, 120.92, 119.20, 117.31, 116.83, 111.91, 111.21, 107.46, 67.85, 55.65, 45.56, 27.43, 25.55, 17.59. Anal. Calcd. for $C_{31}H_{31}N_7O_3$: C, 67.74; H, 5.69; N, 17.84. Found: C,

67.49; H, 5.88; N, 18.13. HRMS (ESI) *m*/*z* $(M+H)^+$ calcd. for $C_{31}H_{32}N_7O_3^+$: 550.2567; found: 550.2562.

*4.1.2.11. 3-[4-(1H-Imidazol-1-yl)butoxy]-4-nitro-N-[4-methyl-3-[[4-(pyridin-3-yl)pyrimidin-2-yl]amino]phenyl]benzamide (**6k**).*

Yellow solid; mp 103.2–105.4 °C; yield 38%. IR (KBr) cm^{-1} 3420, 3406, 2936, 1664, 1582, 1526, 1449, 1416, 1235. ^{1}H NMR (DMSO-d_6) δ 10.42 (s, 1H), 9.29 (d, *J* = 2.0 Hz, 1H), 9.01 (s, 1H), 8.68 (dd, *J* = 4.6, 1.6 Hz, 1H), 8.53–8.45 (m, 2H), 8.08 (d, *J* = 1.8 Hz, 1H), 8.02 (d, *J* = 8.4 Hz, 1H), 7.81–7.78 (m, 1H), 7.67–7.63 (m, 2H), 7.56–7.43 (m, 3H), 7.26–7.17 (m, 2H), 6.88 (s, 1H,, 4.28 (t, *J* = 6.0 Hz, 2H), 4.04 (t, *J* = 7.0 Hz, 2H), 2.22 (s, 3H), 1.91–1.80 (m, 2H, CH_2), 1.75–1.65 (m, 2H, CH_2). ^{13}C NMR (DMSO-d_6) δ 163.61, 161.60, 161.10, 159.46, 151.37, 150.87, 148.19, 140.97, 140.10, 137.90, 137.19, 136.57, 134.40, 132.14, 130.15, 128.37, 128.04, 124.89, 123.77, 119.66, 119.16, 117.24, 116.83, 114.25, 107.62, 68.94, 45.44, 27.11, 25.35, 17.64. Anal. Calcd. for $C_{30}H_{28}N_8O_4$: C, 63.82; H, 5.00; N, 19.85. Found: C, 63.55; H, 5.28; N, 20.12. HRMS (ESI) *m*/*z* $(M+H)^+$ calcd. for $C_{30}H_{29}N_8O_4^+$: 565.2312; found: 565.2310.

*4.1.2.12. 4-[4-(1H-Imidazol-1-yl)butoxy]-3-iodo-N-[4-methyl-3-[[4-(pyridin-3-yl)pyrimidin-2-yl]amino]phenyl]benzamide (**6l**).*

Pale yellow solid; mp 108.7–110.8 °C; yield 20%. IR (KBr) cm^{-1} 3435, 3350, 2923, 1658, 1581, 1529, 1449, 1414, 1256, 801. ^{1}H NMR (DMSO-d_6) δ 10.14 (s, 1H), 9.28 (d, *J* = 1.4 Hz, 1H,, 9.00 (s, 1H), 8.69 (dd, *J* = 4.8, 1.4 Hz, 1H), 8.53–8.40 (m, 3H), 8.06–7.97 (m, 2H), 7.66 (s, 1H), 7.55–7.42 (m, 3H), 7.22–7.08 (m, 3H), 6.90 (s, 1H), 4.16–3.99 (m, 4H), 2.22 (s, 3H), 2.06–1.87 (m, 2H), 1.71–1.65 (m, 2H). ^{13}C NMR (DMSO-d_6) δ 163.27, 161.57, 161.15, 159.44, 159.41, 151.34, 148.15, 138.12, 137.75, 137.19, 137.06, 134.37, 132.17, 129.98, 129.77, 128.71, 128.39, 127.56, 123.74, 119.16, 117.22, 116.73, 111.71, 107.49, 86.25, 68.40, 45.57, 27.30, 25.47, 17.60. Anal.

Calcd. for $C_{30}H_{28}IN_7O_2$: C, 55.82; H, 4.37; N, 15.19. Found: C, 55.59; H, 4.68; N, 15.31. HRMS (ESI) *m*/*z* $(M+H)^+$ calcd. for $C_{30}H_{29}IN_7O_2^+$: 646.1427; found: 646.1422.

*4.1.2.13. 3-Bromo-4-[4-(1H-imidazol-1-yl)butoxy]-N-[4-methyl-3-[[4-(pyridin-3-yl)pyrimidin-2-yl]amino]phenyl]benzamide (**6m**).*

White solid; mp 172.1–174.2 °C; yield 22%. IR (KBr) cm^{-1} 3426, 3370, 2932, 1653, 1578, 152, 1497, 1449, 1418, 1264. ^{1}H NMR (DMSO-d_6) δ 10.15 (s, 1H), 9.28 (d, J = 1.6 Hz, 1H), 9.00 (s, 1H), 8.69 (dd, J = 4.6, 1.4 Hz, 1H), 8.53–8.45 (m, 2H), 8.23 (d, J = 2.2 Hz, 1H), 8.06 (d, J = 1.8 Hz, 1H), 7.98 (dd, J = 8.8, 2.2 Hz, 1H), 7.65 (s, 1H), 7.55–7.42 (m, 3H), 7.24–7.19 (m, 3H), 6.89 (s, 1H), 4.18–4.03 (m, 4H), 2.22 (s, 3H), 1.99–1.84 (m, 2H), 1.76–1.66 (m, 2H). ^{13}C NMR (DMSO-d_6) δ 163.29, 161.56, 161.13, 159.41, 157.08, 151.32, 148.15, 137.75, 137.17, 137.02, 134.35, 132.16, 132.14, 129.98, 128.97, 128.38, 128.18, 127.57, 123.71, 119.14, 117.20, 116.72, 112.92, 110.64, 107.48, 68.40, 45.52, 27.21, 25.43, 17.59. Anal. Calcd. for $C_{30}H_{28}BrN_7O_2$: C, 60.21; H, 4.72; N, 16.38. Found: C, 60.49; H, 4.44; N, 16.59. HRMS (ESI) *m*/*z* $(M+H)^+$ calcd. for $C_{30}H_{29}BrN_7O_2^+$: 598.1566; found: 598.1557.

*4.1.2.14. 4-[4-(1H-Imidazol-1-yl)butoxy]-5-methoxy-N-[4-methyl-3-[[4-(pyridin-3-yl)pyrimidin-2-yl]amino]phenyl]benzamide (**6n**).*

Pale yellow solid; mp 156.5–157.9 °C; yield 35%. IR (KBr) cm^{-1} 3556, 3349, 3102, 2934, 1641, 1580, 1528, 1507, 1451, 1262, 1219. ^{1}H NMR (DMSO-d_6) δ10.05 (s, 1H), 9.29 (d, J = 1.6 Hz, 1H), 9.01 (s, 1H), 8.68 (dd, J = 4.8, 1.6 Hz, 1H), 8.53–8.45 (m, 2H), 8.07 (d, J = 2.0 Hz, 1H), 7.66–7.42 (m, 6H), 7.23–7.20 (m, 2H), 7.09 (d, J = 8.6 Hz, 1H), 6.90 (br s, 1H), 4.09–4.02 (m, 4H), 3.84 (s, 3H), 2.23 (s, 3H), 1.91–1.64 (m, 4H). ^{13}C NMR (DMSO-d_6) δ 164.68, 161.57, 161.17, 159.43, 151.74, 151.33, 148.17, 147.49, 137.74, 137.22, 134.38, 132.18, 129.96, 128.34, 127.41, 127.09, 123.74, 121.09, 119.21, 117.32, 116.84, 112.33, 111.08, 107.48, 67.99, 55.70, 45.59, 27.52, 25.67,

17.59. Anal. Calcd. for $C_{31}H_{31}N_7O_3$: C, 67.74; H, 5.69; N, 17.84. Found: C, 68.00; H, 5.44; N, 17.62. HRMS (ESI) *m/z* $(M+H)^+$ calcd. for $C_{31}H_{32}N_7O_3^+$: 550.2567; found: 550.2561.

4.2. Biological evaluation

4.2.1. Preparation of spleen microsomal fractions

HO-1 was obtained from rat spleen as the microsomal fraction prepared by differential centrifugation; the dominance of HO-1 protein in the rat spleen and has been well documented [51]. This particular microsomal preparation was selected in order to use the most native (i.e., closest to *in vivo*) form of HO-1. Spleen (Sprague-Dawley rats) microsomal fractions were prepared according to the procedure outlined by Ryter *et al* [6]. The experiments reported in the present paper complied with current Italian law and met the guidelines of the Institutional Animal Care and Use Committee of MINISTRY OF HEALTH (Directorate General for Animal Health and Veterinary Medicines) (Italy). The experiments were performed in male Sprague-Dawley albino rats (150 g body weight and age 45 d). They had free access to water and were kept at room temperature with a natural photo-period (12 h light-12 h dark cycle). For measuring HO-1 activity, each rat was sacrificed and their spleen was excised and weighed. A homogenate (15%, w/v) of spleens pooled from four rats was prepared in ice-cold HO-homogenizing buffer (50 mM Tris buffer, pH 7.4, containing 0.25 M sucrose) using a Potter-Elvehjem homogenizing system with a Teflon pestle. The microsomal fraction of rat spleen homogenate was obtained by centrifugation at 10,000g for 20 min at 4 °C, followed by centrifugation of the supernatant at 100,000g for 60 min at 4 °C. The 100,000g pellet (microsomes) was resuspended in 100 mM potassium phosphate buffer, pH 7.8, containing 2 mM $MgCl_2$ with a Potter-Elvehjem homogenizing system. The rat spleen microsomal fractions were divided into equal aliquots, placed into microcentrifuge tubes, and stored at –80 °C for up to 2 months. The protein concentration of the microsomal fraction was determined by Lowry method [28].

4.2.2. Preparation of biliverdin reductase

Liver cytosol has been used as a source of biliverdin reductase (BVR). Rat liver was perfused through the hepatic portal vein with cold 0.9% NaCl, then it was cut and flushed with 2×20 mL of ice-cold PBS to remove all of the blood. Liver tissue was homogenized in 3 volumes of a solution containing 1.15% KCl w/v and Tris buffer 20 mM, pH 7.8 on ice. Homogenates were centrifuged at 10,000g, for 20 min at 4 °C. The supernatant was decanted and centrifuged at 100,000g for 1 h at 4 °C to sediment the microsomes. The 100,000g supernatant was saved and then stored in small amounts at –80 °C after its protein concentration was measured.

4.2.3. Measurement of HO-1 enzymatic activities in microsomal fraction of rat spleen

The HO-1 activity was determined by measuring the bilirubin formation using the difference in absorbance at 464 to 530 nm as described by Ryter *et al* [6]. Reaction mixtures (500 µL) consisted of 20 mM Tris-HCl, pH 7.4, (1 mg/mL) microsomal extract, 0.5–2 mg/mL biliverdin reductase, 1 mM NADPH, 2 mM glucose 6-phosphate (G6P), 1 U G6P dehydrogenase, 25 µM hemin, 10 µL of DMSO (or the same volume of DMSO solution of test compounds to a final concentration of 100, 10, and 1 µM). Incubations were carried out for 60 min at 37 °C in a circulating water bath in the dark. Reactions were stopped by adding 1 volume of chloroform. After recovering the chloroform phase, the amount of bilirubin formed was measured with a double-beam spectrophotometer as OD 464-530 nm (extinction coefficient, 40 mM/cm^{-1} for bilirubin). One unit of the enzyme was defined as the amount of enzyme catalyzing the formation of 1 nmol of bilirubin/mg protein/h.

4.2.4. Cell viability

Cell viability was assessed using the XTT assay kit (Thermo Fisher Scientific). Briefly, K562 sensitive or resistant cells were cultured in a 96-well plate in a density of 1×10^4 cells per well in RPMI medium without phenol red. Following 24 h of incubation, various concentrations of compounds were administered for 24 h. Afterwards, 25 µL of XTT test solution were added to each

well. Following 2 h of incubation, absorbance was measured at 450 nm in a microplate spectrophotometer reader (Thermo Labsystems Multiskan).

4.2.5. Cell Cultures and treatments

Ph^+ cell lines K562R were cultured in RPMI-1640 (Sigma, Milan, Italy) with 10% Fetal Bovine Serum (FBS) and 1% penicillin-streptomycin at a final concentration of 15×10^4 cells/mL and were incubated at 37 °C in 5% CO_2. K562R cells were incubated for 24 h either with IM 10 μM alone, or 10 μM hybrid compounds **6a**–**n**.

Lymphocytes collected from healthy volunteers were isolated using lymphocytes specific Ficoll–Paque PLUS (GE healthcare Life Science, Buckinghamshire, UK) and then cultured at 37 °C in 5% CO_2 in RPMI-1640 containing with 10% FBS and 1% Penicillin/Streptomycin and then incubated for 24 h either with IM 10 μM, or 10 μM hybrid compounds **6i**, **6j**, **6k**, **6m** and **6n**.

4.2.6. Immunoblot analysis

Cells were cultured in T75 flasks, washed with PBS and then trypsinized (0.05% trypsin w/v with 0.02% EDTA). The pellets were lysed in buffer (Tris-Cl 50 mM, EDTA 10 mM, Triton X-100 1% v/v, PMSF 1%, pepstatin A 0.05 mM and leupeptin 0.2 mM) and, after mixing with sample loading buffer (Tris-Cl 50 mM, SDS 10% w/v, glycerol 10% v/v, 2-mercaptoethanol 10% v/v and bromophenol blue 0.04%) at a ratio of 4:1, were boiled for 5 min. Samples (20 μg protein) were loaded into 8 or 12% SDS-polyacrylamide (SDS-PAGE) gels and subjected to electrophoresis (120 V, 90 min). The separated proteins were transferred to nitrocellulose membranes (Bio-Rad, Hercules, CA, USA; 1 h, 200 mA). After transfer, the blots were incubated with Li-Cor Blocking Buffer for 1 h, followed by overnight incubation with 1:1,000 dilution of the primary antibodies directed against anti-CrkL and anti-pCrkL purchased from Santa Cruz (Dallas, TX, USA). After washing with TBS, the blots were incubated for 1 h with secondary antibody (1:2,500). Protein detection was carried out using a secondary infrared fluorescent dye-conjugated antibody absorbing

at 800 nm or 700 nm. The blots were visualized using an Odyssey Infrared Imaging Scanner (Li-Cor Science Tec) and quantified by densitometric analysis performed after normalization with CrkL. Results were expressed as fold of increase of arbitrary units (AU) obtained for treated cells respect untreated controls.

4.2.7. Apoptotic K562R cell death

K562R cell apoptosis was analyzed by Muse Cell Analyzer with the Muse Annexin V & Dead Cell kit (MCH100105, Merck Millipore). The whole process of analysis was performed following the instructions of the kit. The percentage of apoptotic and necrotic cells was calculated from each triplicate sample by statistical analysis of the dot plot using Muse 1.1.2 analysis software (Merck Millipore).

4.2.8. Real-time PCR Quantification

Expression of HO-1 and HO-2 and GAPDH were evaluated by real-time PCR. Cultured cell layers in different conditions were rinsed with cold PBS and immediately lysed using Trizol Reagent (Qiagen). Total RNA was isolated, treated with RNase-free DNase I, and quantified by UV spectrophotometry. For RT-PCR analysis of mRNA expression, 1.0 μg of total RNA (in 20 μL reaction volume) was reverse-transcribed using reverse transcriptase (Roche Diagnostic) and oligo-dT primers in a standard reaction. The resultant cDNA was then used as the template for PCR amplification. The quantitative real-time polymerase chain reaction (qRT-PCR) was performed with the TaqMan gene expression assay (HMOX1 Hs00157965_m1; HMOX2 Hs01558390_m1; GAPDH Hs99999905_m1 Life Technologies) on an ABI Prism 7900 sequence analyzer according to the manufacturer's recommended protocol (Applied Biosystems, Foster City, CA, USA). Each reaction was run in triplicate. The comparative threshold cycle (CT) method was used to calculate the amplification fold as specified by the manufacturer. An amount of 10 ng of reverse transcribed RNA samples was amplified by using the TaqMan Universal PCR Master Mix.

4.2.9. Measurement of HO enzymatic activity in K562R cell line

K562R cells were incubated for 24 h either with IM, **1**, and **2** 10 μM, or 10 μM hybrid compounds **6i** and **6j**. Total HO activity in the cell lysate was determined by measuring the bilirubin formation using the difference in absorbance at 464 to 530 nm as described by Ryter *et al* [6]. Reaction mixtures (500 μL) consisted of 20 mM Tris-HCl, pH 7.4, (1 mg/mL) cell lysate, 0.5–2 mg/mL biliverdin reductase, 1 mM NADPH, 2 mM glucose 6-phosphate (G6P), 1 U G6P dehydrogenase, 25 μM hemin, 10 μL of DMSO. Incubations were carried out for 60 min at 37 °C in a circulating water bath in the dark. Reactions were stopped by adding 1 volume of chloroform. After recovering the chloroform phase, the amount of bilirubin formed was measured with a double-beam spectrophotometer as OD 464–530 nm (extinction coefficient, 40 mM/cm^{-1} for bilirubin). One unit of the enzyme was defined as the amount of enzyme catalyzing the formation of 1 nmol of bilirubin/mg protein/h.

4.2.10. ROS measurement

Determination of ROS was performed by using a fluorescent probe 2',7'-dichlorofluorescein diacetate (DCFH-DA), as previously described [52]. The fluorescence [corresponding to the oxidized radical species 2',7'-dichlorofluorescein (DCF)] was spectrofluorometrically monitored (excitation, λ = 488 nm; emission, λ = 525 nm). The total protein content was evaluated for each sample and the results are reported as fluorescence intensity/mg protein.

4.2.11. Statistical analyses

The data are presented as means ±SD for 4 experiments in triplicate. One-way variance analysis and Student's t-test were used where appropriate; $p<0.05$ was regarded as significant.

4.3. Computational methods

All of the compounds were drawn using Marvin Sketch and subjected to a first molecular mechanics energy minimization by Merck molecular force field (MMFF94) optimization using the Marvin Sketch geometrical descriptors plugin [53]. The protonation states of the molecules were calculated assuming a pH of 7. After having obtained the 3D structures for all compounds, the geometry was also optimized at semi-empirical level using the parameterized model number 3 (PM3) semi-empirical Hamiltonian as implemented in MOPAC package (vMOPAC2016) [54–56]. Docking was performed using AutoDock [42] using the default docking parameters, the point charges were initially assigned according to the AMBER14 force field [57], and then damped to mimic the less polar Gasteiger charges used to optimize the AutoDock scoring function. The setup was done with the YASARA molecular modeling program [58,59]. Docking was performed by applying the Lamarckian genetic algorithm (LGA) implemented in AutoDock. The ligand-centered maps were generated by the program AutoGrid with a spacing of 0.375 Å and dimensions that encompass all atoms extending 5 Å from the surface of the ligand. All of the parameters were inserted at their default settings. In the docking tab, the macromolecule and ligand are selected, and GA parameters are set as ga_runs = 100, ga_pop_size = 150, ga_num_evals = 20000000, ga_num_generations = 27000, ga_elitism = 1, ga_mutation_rate = 0.02, ga_crossover_rate = 0.8, ga_crossover_mode = two points, ga_cauchy_alpha = 0.0, ga_cauchy_beta = 1.0, number of generations for picking worst individual = 10. The X-ray crystal structures of the co-crystal HO-1/QC-80 (PDB code 3HOK) and of the crystal structure of the BCR-ABL kinase domain in complex with IM (PDB code 1IEP) were downloaded from the Protein Data Bank (www.rcsb.org). From the crystal structures of the HO-1/QC-80 complex, we retained only the chain B and the prosthetic-heme group. Since water molecules are not directly involved in complex stabilization they were not considered in the docking process. For both proteins, all protein amino acidic residues were kept rigid whereas all single bonds of ligands were treated as full flexible. For molecules **6l** and **6m**, best binding energies for HO-1 were obtained after a Molecular Dynamics (MD) simulation. In these cases, the ligands were first docked into the selected binding sites of HO-1,

after the first docking calculation the best pose was manually selected and then the complex (ligand/HO-1) was minimized toward a MD simulation of 10ns. Finished the MD simulation each ligand was extracted and re-docked into the binding site. The MD simulation was made in explicit water using YASARA as a software. A 10 Å simulation cell (SC) around all atoms was used. YASARA's AMBER 14 [60,61] force field was used for the simulation. Simulation temperature was set at 298 K, the SC was uniformly rescaled to reach a pressure of 1 bar, the pH was set at 7. The simulation was run for 10 ns and single snapshots were recorded every 250 ps. The properties related to ADME of molecules **6i** and **6j** were predicted using PreADMET web-based application (http://preadmet.bmdrc.kr) [62], the in silico toxicity study for the same set of molecules was performed using DataWarrior (V4.7.2) software.

Acknowledgement

This work was supported by 1) Research Funding for University (Piano per la Ricerca 2016–2018, project code 57722172107) and 2) Project authorized by the Ministry of Health (Directorate General for Animal Health and Veterinary Medicines) "Dosing of enzymatic activities in rat microsomes" (2018–2022) (project code 02769.N.VLY).

Supplementary data

This material is available free of charge via the Internet at http://dx.doi.org/. Synthesis of bromobutoxybenzoates **3a**–**n**; synthesis of methyl imidazolylbutoxybenzoates **4a**–**n**; docked poses inside HO-1 of compounds **6a**, **6f**, **6g**, **6j**, **6l**, and **6m** (Figures S3–S9); docked poses inside BCR-ABL of compounds **6a**, **6g**, **6i**, **6j** and **6l** (Figures S10–S15); correlation between the calculated free energies of binding and percentage of inhibitory efficiency for BCR-ABL (Figure S16 B); ^{1}H NMR and ^{13}C NMR spectra of compounds **6a–n**.

References

[1] R.Tenhunen, H.S. Marver, R.Schmid, The enzymatic conversion of heme to bilirubin by microsomal heme oxygenase, Proc. Natl. Acad. Sci. U. S. A. 61 (1968) 748–755.

[2] M.D. Maines, The heme oxygenase system: past, present, and future, Antioxid. Redox Signal. 6 (2004) 797–801.

[3] T. Yoshida, C.T. Migita, Mechanism of heme degradation by heme oxygenase, J. Inorg. Biochem. 82 (2000) 33–41.

[4] V. Pittalà, L. Vanella, L. Salerno, C. Di Giacomo, R. Acquaviva, M. Raffaele, G. Romeo, M.N. Modica, O. Prezzavento, V.Sorrenti, Novel caffeic acid phenethyl ester (Cape) analogues as inducers of heme oxygenase-1, Curr. Pharm. Des. 23 (2017) 2657–2664.

[5] V. Pittalà, L. Vanella, L. Salerno, G. Romeo, A. Marrazzo, C. Di Giacomo, V. Sorrenti, Effects of polyphenolic derivatives on heme oxygenase-system in metabolic dysfunctions, Curr. Med. Chem. 25 (2017) 1577–1595.

[6] S.W. Ryter, J. Alam, A.M. Choi, Heme oxygenase-1/carbon monoxide: from basic science to therapeutic applications, Physiol. Rev. 86 (2006) 583–650.

[7] Grochot-Przeczek, J. Dulak, A. Jozkowicz, Haem oxygenase-1: non-canonical roles in physiology and pathology, Clinical Science 122 (2012) 93–103.

[8] E. Amata, V. Pittalà, A. Marrazzo, C. Parenti, O. Prezzavento, E. Arena, S.M. Nabavi, L. Salerno, Role of the Nrf2/HO-1 axis in bronchopulmonary dysplasia and hyperoxic lung injuries, Clinical Science 131 (2017) 1701–1712.

[9] M. Nitti, S. Piras, U.M. Marinari, L. Moretta, M.A Pronzato, A.L. Furfaro, HO-1 Induction in Cancer Progression: A matter of cell adaptation, Antioxidants 6 (2017) pii E29.

[10] L.Y. Chau, Heme oxygenase-1: emerging target of cancer therapy, J. Biomed. Sci. (2015) 22:22.

[11] K.V. Gleixner, M. Mayerhofer, A. Vales, A. Gruze, G. Hormann, S. Cerny-Reiterer, E. Lackner, E. Hadzijusufovic, H. Herrmann, A.K. Iyer, M.T. Krauth, W.F. Pickl, B. Marian, R. Panzer-Grumayer, C.Sillaber, H. Maeda, C. Zielinski, P.Valent, Targeting of Hsp32 in solid tumors

and leukemias: a novel approach to optimize anticancer therapy, Curr. Cancer Drug Targets 9 (2009) 675–689.

[12] G. Li Volti, D. Tibullo, L. Vanella, C. Giallongo, F. Di Raimondo, S. Forte, M. Di Rosa, S.S. Signorelli, I. Barbagallo, The heme oxygenase system in hematological malignancies, Antioxid. Redox Signal. 27 (2017) 363–377.

[13] L. Salerno, G. Romeo, M.N. Modica, E. Amata, V. Sorrenti, I. Barbagallo, V. Pittalà, Heme oxygenase-1: A new druggable target in the management of chronic and acute myeloid leukemia, Eur. J. Med. Chem. 142 (2017) 163–178.

[14] J.V. Melo, D.J. Barnes, Chronic myeloid leukaemia as a model of disease evolution in human cancer, Nat. Rev. Cancer 7 (2007) 441–453.

[15] X. An, A.K. Tiwari, Y. Sun, P.R. Ding, C.R.Jr. Ashby, Z.S. Chen, BCR-ABL tyrosine kinase inhibitors in the treatment of Philadelphia chromosome positive chronic myeloid leukemia: a review, Leuk. Res. 34 (2010) 1255–1268.

[16] S.G. O'Brien, F. Guilhot, R. A. Larson, I. Gathmann, M. Baccarani, F. Cervantes, J.J. Cornelissen, T. Fischer, A. Hochhaus, T. Hughes, K. Lechner, J.L. Nielsen, P. Rousselot, J. Reiffers, G. Saglio, J. Shepherd, B. Simonsson, A. Gratwohl, J.M. Goldman, H. Kantarjian, K. Taylor, G. Verhoef, A.E. Bolton, R. Capdeville, B.J. Druker, I. Investigators, Imatinib compared with interferon and low-dose cytarabine for newly diagnosed chronic-phase chronic myeloid leukemia, N. Engl. J. Med. 348 (2003) 994–1004.

[17] J. V. Melo, C. Chuah, Resistance to imatinib mesylate in chronic myeloid leukaemia, Cancer Lett. 249 (2007) 121–132.

[18] Pasic, J.H. Lipton, Current approach to the treatment of chronic myeloid leukaemia, Leuk. Res. 55 (2017) 65–78.

[19] S. Roumiantsev, N.P. Shah, M.E. Gorre, J. Nicoll, B.B. Brasher, C.L. Sawyers, R.A. Van Etten, Clinical resistance to the kinase inhibitor STI-571 in chronic myeloid leukemia by mutation

of Tyr-253 in the Abl kinase domain P-loop, Proc. Natl. Acad. Sci. U. S. A. 99 (2002) 10700–10705.

[20] M. E. Gorre, M. Mohammed, K. Ellwood, N. Hsu, R. Paquette, P.N. Rao, C.L Sawyers, Clinical resistance to STI-571 cancer therapy caused by BCR-ABL gene mutation or amplification, Science 293 (2001) 876–880.

[21] M.E. Irwin, N. Rivera-Del Valle, J. Chandra, Redox control of leukemia: from molecular mechanisms to therapeutic opportunities, Antioxid. Redox Signal. 18 (2013) 1349–1383.

[22] M. Mayerhofer, S. Florian, M.T. Krauth, K.J. Aichberger, M. Bilban, R. Marculescu, D. Printz, G. Fritsch, O. Wagner, E. Selzer, W.R. Sperr, P. Valent, C. Sillaber, Identification of heme oxygenase-1 as a novel BCR/ABL-dependent survival factor in chronic myeloid leukemia, Cancer Res. 64 (2004) 3148–3154.

[23] D. Tibullo, I. Barbagallo, C. Giallongo, P. La Cava, N. Parrinello, L.;Vanella, F. Stagno, G.A. Palumbo, G. Li Volti, F. Di Raimondo, Nuclear translocation of heme oxygenase-1 confers resistance to imatinib in chronic myeloid leukemia cells, Curr. Pharm. Des. 19 (2013) 2765–2770.

[24] L. Salerno, V. Pittalà, G. Romeo, M.N. Modica, M.A. Siracusa, C. Di Giacomo, R. Acquaviva, I. Barbagallo, D. Tibullo, V. Sorrenti, Evaluation of novel aryloxyalkyl derivatives of imidazole and 1,2,4-triazole as heme oxygenase-1 (HO-1) inhibitors and their antitumor properties. Bioorg. Med. Chem. 21 (2013) 5145–5153.

[25] Loboda, A. Jozkowicz, J. Dulak, HO-1/CO system in tumor growth, angiogenesis and metabolism - Targeting HO-1 as an anti-tumor therapy, Vasc. Pharmacol. 74 (2015) 11–22.

[26] L. Salerno, V. Pittalà, G. Romeo, M.N. Modica, A. Marrazzo, M.A. Siracusa, V. Sorrenti, C.Di Giacomo, L. Vanella, N.N. Parayath, K. Greish, Novel imidazole derivatives as heme oxygenase-1 (HO-1) and heme oxygenase-2 (HO-2) inhibitors and their cytotoxic activity in human-derived cancer cell lines, Eur. J. Med. Chem. 96 (2015) 162–172.

[27] R. G. Fu, Y. Sun, W.B. Sheng, D.F. Liao, Designing multi-targeted agents: An emerging anticancer drug discovery paradigm, Eur. J. Med. Chem. 136 (2017) 195–211.

[28] V. Sorrenti, S. Guccione, C. Di Giacomo, M.N. Modica, V. Pittalà, R. Acquaviva, L. Basile, M. Pappalardo, L.Salerno, Evaluation of imidazole-based compounds as heme oxygenase-1 inhibitors, Chem. Biol. Drug Des. 80 (2012) 876–886.

[29] V. Pittalà, L. Salerno, G. Romeo, M.N. Modica, M.A. Siracusa, A focus on heme oxygenase-1 (HO-1) inhibitors, Curr. Med. Chem. 20 (2013) 3711–3732.

[30] M.N. Rahman, D. Vukomanovic, J.Z. Vlahakis, W.A.;Szarek, K. Nakatsu, Z. Jia, Structural insights into human heme oxygenase-1 inhibition by potent and selective azole-based compounds, J. R. Soc. Interface 10 (2013) 20120697.

[31] E. Amata, A. Marrazzo, M. Dichiara, M.N. Modica, L. Salerno, O. Prezzavento, G. Nastasi, A. Rescifina, G. Romeo, V. Pittalà, Heme oxygenase database (HemeOxDB) and QSAR analysis of isoform 1 inhibitors, ChemMedChem 12 (2017) 1873–1881.

[32] E. Amata, A. Marrazzo, M. Dichiara, M.N. Modica, L. Salerno, O. Prezzavento, G. Nastasi, A. Rescifina, G. Romeo, V. Pittalà, Comprehensive data on a 2D-QSAR model for Heme Oxygenase isoform 1 inhibitors, Data in brief 15 (2017) 281–299.

[33] N. Shalmali, M.R. Ali, S. Bawa, Imidazole: An essential edifice for the identification of new lead compounds and drug development, Mini Rev. Med. Chem. 18 (2018) 142–163.

[34] S. Ferla, A.S; Aboraia, A. Brancale, C. J. Pepper, J. Zhu, J. T. Ochalek, H. F. DeLuca, C. Simons, Small-molecule inhibitors of 25-hydroxyvitamin D-24-hydroxylase (CYP24A1): synthesis and biological evaluation, J. Med. Chem. 57 (2014) 7702–7715.

[35] Q. Su, S. Ioannidis, C. Chuaqui, L. Almeida, M. Alimzhanov, G. Bebernitz, K. Bell, M. Block, T. Howard, S. Huang, D. Huszar, J.A. Read, C. Rivard Costa, J. Shi, M. Su, M. Ye, M. Zinda, Discovery of 1-methyl-1H-imidazole derivatives as potent Jak2 inhibitors, J. Med. Chem. 57 (2014) 144–158.

[36] M. Hum, B.E. McLaughlin, G. Roman, J. Z. Vlahakis, W.A. Szarek, K. Nakatsu, The effects of azole-based heme oxygenase inhibitors on rat cytochromes P450 2E1 and 3A1/2 and human cytochromes P450 3A4 and 2D6, J. Pharmacol. Exp. Ther. 334 (2010) 981–987.

[37] C-R. Lee, J-A. Kang, H-E. Kim, Y. Choi, T. Yang, S-G. Park, Secretion of IL-1β from imatinib-resistant chronic myeloid leukemia cells contributes to BCR-ABL mutation independent imatinib resistance, FEBS Lett. 590 (2016) 358–368.

[38] P. La Rosee, S. Holm-Eriksen, H. Konig, N. Hartel, T. Ernst, J. Debatin, M.C. Mueller, P. Erben, A. Binckebanck, L. Wunderle, Y. Shou, M. Dugan, R. Hehlmann, O.G. Ottmann, A.Hochhaus, Phospho-CRKL monitoring for the assessment of BCR-ABL activity in imatinib-resistant chronic myeloid leukemia or Ph+ acute lymphoblastic leukemia patients treated with nilotinib, Haematologica 93 (2008) 765–769.

[39] D. Datta, P. Banerjee, M. Gasser, A.M. Waaga-Gasser, S. Pal, CXCR3-B can mediate growth-inhibitory signals in human renal cancer cells by down-regulating the expression of heme oxygenase-1, J. Biol. Chem. 285 (2010) 36842–36848.

[40] Y. Shan, J. Pepe, T.H. Lu, K.K. Elbirt, R.W. Lambrecht, H.L. Bonkovsky, Induction of the heme oxygenase-1 gene by metalloporphyrins, Arch. Biochem. Biophys. 380 (2000) 219–227.

[41] B. Nagar, W.G. Bornmann, P. Pellicena, T. Schindler, D.R. Veach, W.T. Miller, B. Clarkson, J. Kuriyan, Crystal structures of the kinase domain of c-Abl in complex with the small molecule inhibitors PD173955 and imatinib (STI-571), Cancer Res. 62 (2002) 4236–4243.

[42] G. M. Morris, R. Huey, W. Lindstrom, M.F. Sanner, R.K. Belew, D.S. Goodsell, A.J. Olson, AutoDock4 and AutoDockTools4: Automated docking with selective receptor flexibility, J. Comput. Chem. 30 (2009) 2785–2791.

[43] L. Salerno, E. Amata, G. Romeo, A. Marrazzo, O. Prezzavento, G. Floresta, V. Sorrenti, I. Barbagallo, A. Rescifina, V. Pittalà, Potholing of the hydrophobic heme oxygenase-1 western region for the search of potent and selective imidazole-based inhibitors, Eur. J. Med. Chem. 148 (2018) 54–62.

[44] K.F. Greish, L. Salerno, R. Al Zahrani, E. Amata, M.N. Modica, G. Romeo, A. Marrazzo, O. Prezzavento, V. Sorrenti, A. Rescifina, G. Floresta, S. Intagliata, V. Pittalà, Novel structural

insight into inhibitors of heme oxygenase-1 (HO-1) by new imidazole-based compounds: biochemical and in vitro anticancer activity evaluation, Molecules, 2018, 23, 1209.

[45] G. Floresta, E. Amata, M. Dichiara, A. Marrazzo, L. Salerno, G. Romeo, O. Prezzavento, V. Pittalà, A. Rescifina, Identification of potentially potent heme oxygenase 1 inhibitors through 3D-QSAR coupled to scaffold-hopping analysis, ChemMedChem. 13 (2018) 1336–1342.

[46] Y.L. Lin, Y. Meng, W. Jiang, B. Roux, Explaining why Gleevec is a specific and potent inhibitor of Abl kinase, Proc. Natl. Acad. Sci. U. S. A. 110 (2013) 1664–1669.

[47] Z. Peng, D.S. Maxwell, D. Sun, B.A. Bhanu Prasad, A. Pal, S. Wang, J. Balatoni, P. Ghosh, S. T. Lim, A. Volgin, A. Shavrin, M.M. Alauddin, J.G. Gelovani, W.G. Bornmann, Imatinib analogs as potential agents for PET imaging of Bcr-Abl and c-KIT expression at a kinase level, Bioorg. Med. Chem. 22 (2014) 623–632.

[48] X. Pan, J. Dong, H. Gao, F. Wang, Y. Zhang, S. Wang, J. Zhang, Design, synthesis and biological evaluation of pyridin-3-yl pyrimidines as potent Bcr-Abl inhibitors, Chem. Biol.& Drug Des. 83 (2014) 592–599.

[49] T. Sander, J. Freyss, M. Von Korff, C. Rufener, DataWarrior: an open-source program for chemistry aware data visualization and analysis, J. Chem. Inf. Model. 55 (2015) 460-473.

[50] Barbagallo, C. Giallongo, G. Li Volti, A. Distefano, G. Camiolo, M. Raffaele, L. Salerno, V. Pittalà, V. Sorrenti, R. Avola, M. Di Rosa, L. Vanella, F. Di Raimondo, D. Tibullo, Heme oxygenase inhibition sensitizes neuroblastoma cells to carfilzomib, Mol. Neurobiol. (2018) in press, doi: 10.1007/s12035-018-1133-6.

[51] J.Z. Vlahakis, C. Lazar, G. Roman, D. Vukomanovic, K. Nakatsu, W.A. Szarek, Heme oxygenase inhibition by alpha-(1H-imidazol-1-yl)-omega-phenylalkanes: effect of introduction of heteroatoms in the alkyl linker, ChemMedChem 7 (2012) 897–902.

[52] R. Acquaviva, C. Di Giacomo, V. Sorrenti, F. Galvano, R. Santangelo, V. Cardile, S. Gangia, N. D'Orazio, N.G. Abraham, L.Vanella, Antiproliferative effect of oleuropein in prostate cell lines, Int. J. Oncol. 41 (2012) 31–38.

[53] E. Chatelain, Chagas disease research and development: Is there light at the end of the tunnel? Comput. Struct. Biotechnol. J. 15 (2017) 98–103.

[54] J.J. Stewart, Optimization of parameters for semiempirical methods IV: extension of MNDO, AM1, and PM3 to more main group elements, J. Mol. Model. 10 (2004) 155–164.

[55] C. Aleman, F.J. Luque, M. Orozco, Suitability of the Mp3-derived Molecular electrostatic potentials, J. Comput. Chem. 14 (1993) 799–808.

[56] MOPAC2016 Stewart Computational Chemistry, http://OpenMOPAC.net 2016.

[57] Y. Duan, C. Wu, S. Chowdhury, M.C. Lee, G. Xiong, W. Zhang, R. Yang, P. Cieplak, R. Luo, T. Lee, J. Caldwell, J. Wang, P. Kollman, A point-charge force field for molecular mechanics simulations of proteins based on condensed-phase quantum mechanical calculations, J. Comput. Chem. 24 (2003) 1999–2012.

[58] E. Krieger, G.Vriend, YASARA View - molecular graphics for all devices - from smartphones to workstations, Bioinformatics 30 (2014) 2981–2982.

[59] E. Krieger, G. Vriend, New ways to boost molecular dynamics simulations, J. Comput. Chem. 36 (2015) 996–1007.

[60] J.W. Ponder, D.A Case, Force fields for protein simulations, Adv. Protein Chem. 66 (2003) 27–85.

[61] V. Hornak, R. Abel, A. Okur, B. Strockbine, A. Roitberg, C. Simmerling, Comparison of multiple Amber force fields and development of improved protein backbone parameters, Proteins 65 (2006) 712–725.

[62] S.K. Lee, I.H. Lee, H.J. Kim, G.S. Chang J.E. Chung, K.T. No. The Pre ADME Approach: Web-based program for rapid prediction of physico-chemical, drug absorption and drug-like properties. In: Designing drugs and crop protectants: processes, problems and solutions. Edited by M.G.Ford, 2003 Malden, MA, Blackwell Pub.